Graduate Theses and Dissertations   Graduate School

2014

31P Dynamic Nuclear Polarization Applied to Dimethyl Methyl Phphonate for Functional Imaging and Spectroscopic Studies

Roha Afzal
University of South Florida, roha@mail.usf.edu

Follow this and additional works at: http://scholarcommons.usf.edu/etd

Part of the Biomedical Engineering and Bioengineering Commons

^{31}P Dynamic Nuclear Polarization Applied to Dimethyl Methyl Phosphonate for Functional

Imaging and Spectroscopic Studies

by

Roha Afzal

A thesis submitted in the partial fulfilment
of the requirements for the degree of
Master of Science in Biomedical Engineering
Department of Chemical and Biomedical Engineering
College of Engineering
University of South Florida

Major Professor: Robert J. Gillies, Ph.D.
Robert D. Frisina, Ph.D.
Anna Pyayt, Ph.D.

Date of Approval:
July 7, 2014

Keywords: Perfusion, Hyperpolarization, NMR, OX063, TEMPO

Dedication

I want to dedicate this research work to my mother, grandparents and brothers who have supported me through thick and thin in life.

Acknowledgments

Table of Contents

ii

List of Tables

List of Figures

Abstract

In the recent years, Dynamic Nuclear Polarization (DNP) has emerged as a very promising technique for enhancing the sensitivity of the magnetic resonance spectroscopy and imaging (MRSI). A number of nuclei, namely ^{13}C, ^{15}N, ^{29}Si, ^{89}Y, and ^{129}Xe, have been successfully polarized and a few of them have been employed in the in-vivo studies for functional imaging and metabolism. Hyperpolarized ^{13}C-labeled compounds have wide applications in the metabolic and perfusion studies and can be used for early stage disease diagnosis, response to treatment, prognosis etc. DNP has been demonstrated in the ^{31}P nucleus in nucleotides triphosphates as an application for the structural analysis and identification techniques. In this work, ^{31}P DNP has been successfully applied, optimized and demonstrated in Dimethyl Methyl Phosphonate (DMMP) for the first time. DMMP is a freely diffusible tracer and hyperpolarized DMMP can potentially be used in the perfusion studies using MR imaging and spectroscopic techniques. The polarization buildup and signal enhancements were optimized for two different radicals, a nitroxyl radical TEMPO and a trityl radical OX063. Microwave frequency sweeps were done for both the radicals to find out the optimum frequencies for maximum polarization, Maximum signal enhancement (≈ 2300 folds) and maximum percent polarization buildup (2.15%) were achieved by polarizing DMMP with the radical OX063 at the microwave frequency of 94.080 GHz with a glassing matrix containing D_2O and glycerol and by using D_2O in the dissolution step. DMMP was hyperpolarized at the optimum conditions and injected in a mouse for in-vivo spectroscopy and imaging. The results show that hyperpolarized DMMP is a potential candidate for functional imaging and metabolism.

Chapter 1: Introduction

DNP is evolving as a broadly applicable technique to enhance signal strengths and sensitivity in solid state and solution magnetic resonance spectroscopy and imaging (MRSI) experiment. The reduction of acquisition times associated with DNP-MRSI experiments makes it possible to study reaction dynamics and transient processes. Magnetic resonance imaging of different endogenous and exogenous molecules in living tissues and organisms is a promising tool for metabolism, bioenergetics and perfusion studies and can play an important role in early stage disease diagnosis, response to treatment and prognosis. A number of ^{13}C labeled compounds have been successfully polarized and imaged in-vivo and in-vitro. The application of hyperpolarized compounds for cancer metabolic imaging was first shown by Golman [28, 29]. Since then a number of compounds have been successfully hyperpolarized and employed in preclinical studies for diagnosis, response to treatment and progression of cancer [8]. Hyperpolarized [1-^{13}C] pyruvate has been used to study glycolysis, therapy response and LDH activity in tumor cells [42] [43] [44] [45]. Hyperpolarized [1-^{13}C] lactate has been employed in LDH activity studies. Hyperpolarized ^{13}C bicarbonate has been used to determine the pH of the tumor microenvironment [27]. Hyperpolarized [1-^{13}C] urea has been employed in perfusion studies [47].

^{15}N-labeled choline has also been successfully polarized and used in phospholipid metabolic studies for cancer detection and response assessment [26].

Some other nuclei that have been successfully hyperpolarized through DNP and have potential applications in biomedical imaging include ^{29}Si [23], ^{89}Y [46], and ^{129}Xe.

To date, the application of DNP has been mainly limited to the above mentioned nuclei. This work presents the first application of ^{31}P DNP applied to phosphonates. I have successfully hyperpolarized DMMP and shown that it could be a potential exogenous agent for hyperpolarized imaging in-vivo. DMMP is a freely diffusible tracer and earlier works by Dr. Gillies have shown the application of this compound to measure the cell volumes in vivo [24]. The results of this research work indicate that hyperpolarized DMMP is a potential exogenous tracer for magnetic resonance perfusion studies.

^{31}P dynamic nuclear hyperpolarization has been applied to deoxynucleotides, triphosphates and oligonucleotides for NMR studies of biomolecules such as DNA, RNA, proteins, for structural identification purposes [25].

Perfusion imaging studies can reveal information about the abnormalities which could be associated with conditions like stroke, myocardial ischemia, cancer and pulmonary embolism. These diseases can cause changes in the local tissue perfusion and perfusion imaging can play an important role in the management and control of these and other related conditions.

Normally, perfusion imaging studies like Dynamic Contrast Enhanced (DCE) MRI, involve the use of exogenous tracers to track the flow of blood. This is a powerful widely applied method that tracks flow and permeability however, arterial spin labeling (ASL) makes use of the nuclear magnetization of the blood [30].

Various techniques for the perfusion imaging include positron emission tomography (PET), single photon emission computed tomography (SPECT), computed tomography (CT), magnetic resonance (MR). PET perfusion imaging techniques employ ^{15}O labeled water [31] or ^{11}C labeled compounds [32] as freely diffusible agents. These techniques provide very good quantification but

the spatial and temporal resolution obtained with this technique are limited. Moreover, due to that short lived nature of the radioisotope employed as the freely diffusible tracers, a cyclotron is required to be present nearby. SPECT perfusion imaging techniques use contrast agents as ^{99m}Tc-hexamethylpropyleneamine oxime (Tc-HMPAO) [33]. SPECT methods involving the use of this freely diffusible agent have the disadvantage of poor spatial resolution and a compromised ability of assessing the flow by this agent [34]. CT based methods make use of the contrast agents like iodine [35] and xenon [36]. The main challenges associated with these schemes is the partial permeability of iodinated compounds and exposure to high dose radiations [37]. Most common MR based perfusion imaging technique is the relaxivity based dynamic contrast enhancement (DCE-MRI) which has been widely used to investigate angiogenesis and response to angiogenic therapy. The most common and widely used contrast for these studies is Gd-diethylenetriamine pentaacetic acid (Gd-DTPA) [41]. Other MR based perfusion imaging studies employ gadolinium based partially permeable contrast agents which form the basis of dynamic susceptibility contrast (DSC) techniques [38]. Other freely diffusible tracers for MR perfusion imaging methods include ^{17}O labeled water [39], deuterium [40] and the nuclear magnetization of blood in the case of ASL [30]. Although, ASL methods provide better temporal and spatial resolution as compared to the PET methods, low signal to noise ratio (SNR) and short lifetime of the spin label render this technique somewhat limited in its applicability.

Therefore, alternative methods involving freely diffusible agents that could provide better spatial and temporal resolution, more and slowly decaying perfusion induced signal would be advantageous for perfusion studies. Hyperpolarization provides a higher SNR and an ample amount of signal and thus provides an advantageous alternative technique for perfusion imaging.

Moreover, one other benefit of the hyperpolarized DMMP is its use with other phosphonates e.g., 3-aminopropylphosphonic acid (3-APP), an intracellular pH indicator, for the simultaneous characterization of blood perfusion, cell volume and cell pH. This technique is potentially beneficial for the hyperpolarized imaging of different biomarkers using a single nucleus.

Chapter 2: Theoretical Background of Nuclear Magnetic Resonance

2.1 Nuclear Spin and Spin Angular Momentum

The concept that nuclei possess properties such as angular momentum and a magnetic moment was first introduced by Pauli in 1924 to explain the hyperfine structure of atomic spectra. After the introduction of the concept of the electronic spin by Uhlenbeck and Goudsmit in 1925, which helped explain many unknown and mysterious details of the spectra, scientists deemed it suitable to attribute to the nucleus a mechanical spin by connecting the magnetic moment of the nuclei to the rotating charges. Spin is an intrinsic property of nuclei and a purely quantum mechanical concept. The properties and behavior under a rotation of the coordinate system of spin angular momentum is similar to the angular momentum. While the orbital quantum number can assume only the integer values, it is possible for the spin quantum number to also have half integer values. Elementary particles with integer spin are termed Bosons and are generally responsible for forces whereas the particles that have half integer spins have mass and make up matter. They are termed Fermions. It has been found that the spin for neutrons and protons is ½, just as for the electrons. Since, the nuclear spin I is composed of the spins of the protons and neutrons and their angular momenta in the nucleus, I must be an integer or a half integer depending upon whether the number of the elementary particles is even or odd respectively. The square of the spin angular momentum $\vec{I}$ has eigenvalues $I(I+1)\,\hbar^2$. The spin angular momentum $\vec{I}$ for a particle or a nucleus having a spin quantum number I is given by the following equation:

$$\text{Magnitude of the spin angular momentum} = \hbar\sqrt{I(I+1)} \qquad 2.1$$

2.2 Nuclear Magnetization

Nuclear magnetism of a nuclear spin system arises from the collective effect of the microscopic magnetic fields associated with nuclear spins. From a classical point of view, the existence of nuclear magnetism can be explained by the fact that a nucleus has electrical charges and it rotates around its own axis if it has a non-zero spin. Therefore, like any spinning charged object, it creates a magnetic field around it. It is represented by a vector quantity $\vec{\mu}$ and is termed nuclear magnetic dipole moment or magnetic moment. As the magnetic moment of a nucleus is closely related to its spin angular momentum and is directly proportional to it, it is given by the following equation:

$$\vec{\mu} = \gamma \vec{I} = \gamma \hbar \sqrt{I(I+1)} \qquad 2.2$$

The symbol γ represents the gyromagnetic ratio of the nuclei. Depending on the gyromagnetic ratio, the magnetic moment of the nuclei is either parallel (for positive γ) or antiparallel (for negative γ) to the spin angular momentum, and is a property of a nucleus that describes the ratio of its magnetic moment to its angular momentum.

2.3 Space Quantization of Spin Angular Momentum in an External Magnetic Field

When placed in an external magnetic field $\vec{B}_0$, the directions of the individual spins and the angular momentum becomes quantized by a quantity called magnetic quantum number, m. The magnetic quantum number m has $2I+1$ values in integral steps between $+I$ and $-I$:

$$m = I, I\text{-}1, I\text{-}2, \dots -I+1, -I \qquad 2.3$$

If the external magnetic field is aligned along z-axis, the z component of the magnetic moment aligns with the z axis as well and is given by:

$$\mu_z = \gamma m \hbar \qquad 2.4$$

6

For example, the spin angular momentum of a spin ½ nucleus has two permitted directions in space, $I_z = \pm \frac{1}{2} \hbar$ while a nucleus with a spin quantum number 1 have 3 permitted directions in space , $I_z = 0, \pm \hbar$. Fig 1 shows the space quantization of the angular momentum of these two nuclei.

From the Hamiltonian operator, the total energy of the system may be obtained in the presence of an external magnetic field $\vec{B}_0$ and is given by:

$$E = -\vec{\mu} \cdot \vec{B}_0 \qquad \qquad 2.5$$

In the absence of an external magnetic field, all $2I+1$ orientations of a nucleus are degenerate. In other words, they have the same energy, where this degeneracy is removed in the presence of an external magnetic field.

If the external magnetic field is directed along z direction, the energy of the Zeeman interaction would then be given by:

$$E = -\hbar \gamma B_0 \vec{I}_z \qquad \qquad 2.6$$

Note that there are $2I +1$ available energy levels along the z-axis which are equally spaced with the energy gap given by the equation:

$$\Delta E = \hbar \gamma B_o \qquad \qquad 2.7$$

2.4 Larmor Precession Around the External Magnetic Field

Any system that possesses an angular momentum $\vec{J}$ and a magnetic moment $\vec{\mu}$ reorients itself when placed in an external magnetic field $\vec{B}_0$. This theory was given by Guttinger and Majorana [22]. The frequency of this precession, termed Larmor frequency is given by:

$$\omega_o = \gamma B_0 \qquad\qquad\qquad 2.8$$

this precession of the magnetic moment $\vec{\mu}$ around $\vec{B}_0$ resembles the wobbling of a spinning top around the gravitational axis.
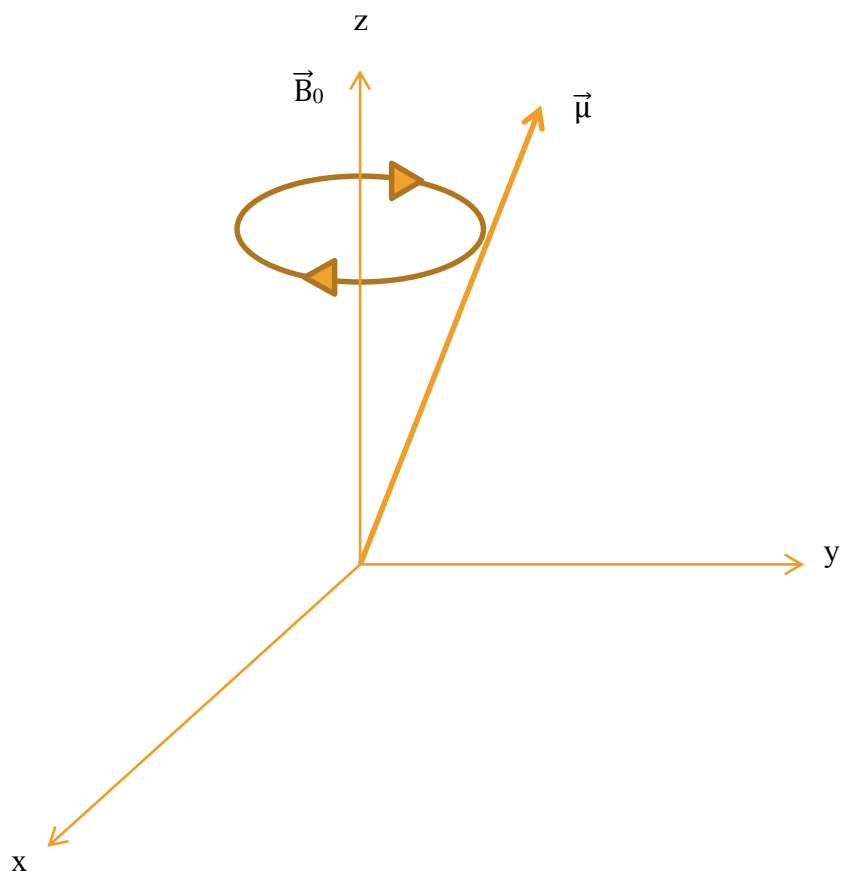
Figure 2.1 The precession of magnetic moment $\vec{\mu}$ around the magnetic field $\vec{B}_0$ in the direction of the z axis.

2.5 Polarization; Populations of the Energy Levels

In the presence of an external magnetic field, magnetic nuclei arrange themselves amongst the $2I+1$ available energy levels according to the Boltzmann distribution. For example, a nucleus with spin quantum number ½ has two possible energy states, namely α and β corresponding to m of +1/2 and -1/2 respectively.

The Zeeman energy involved in magnetic resonance is relatively small relative to other forms of spectroscopy, such as optical for example. The energy level α has a slightly lower energy associated with it as compared to the energy level β and hence is slightly more populated. However, at temperatures significantly higher than zero Kelvin, the system has enough energy as to equally populate both states. Individual spins in the system can alternate between the two states, but the polarization (or magnetization) of the whole system is obtained from a special form of the Boltzmann distribution for spin ½ particles in a magnetic field, which is:

$$P = \frac{N_\alpha - N_\beta}{N_\alpha + N_\beta} = \tanh \frac{h\gamma B_0}{2k_B T} \qquad 2.9$$

where γ is the gyromagnetic ratio of the nucleus, B_0 is the static magnetic field strength, $\hbar$ is Planck's constant divided by 2π, k_B is the Boltzmann constant and T is the temperature in Kelvin. N_α and N_β are the populations of the energy levels α and β respectively. It is evident from the above equation that the polarization varies with the strength of the magnetic field and temperature. Figure 2.1 shows the trend of the population distribution with increasing magnetic field at ambient temperature of 298K. The gyromagnetic ratios for the selected spin ½ nuclei are given in table 2.1.

Table 2.1 Gyromagnetic ratios for selected spin 1/2 species

Species	Gyromagnetic ratios (MHz/T)
^{31}P	17.235
^{13}C	10.705
^1H	42.576
Electron	-2.8025 x 10^4
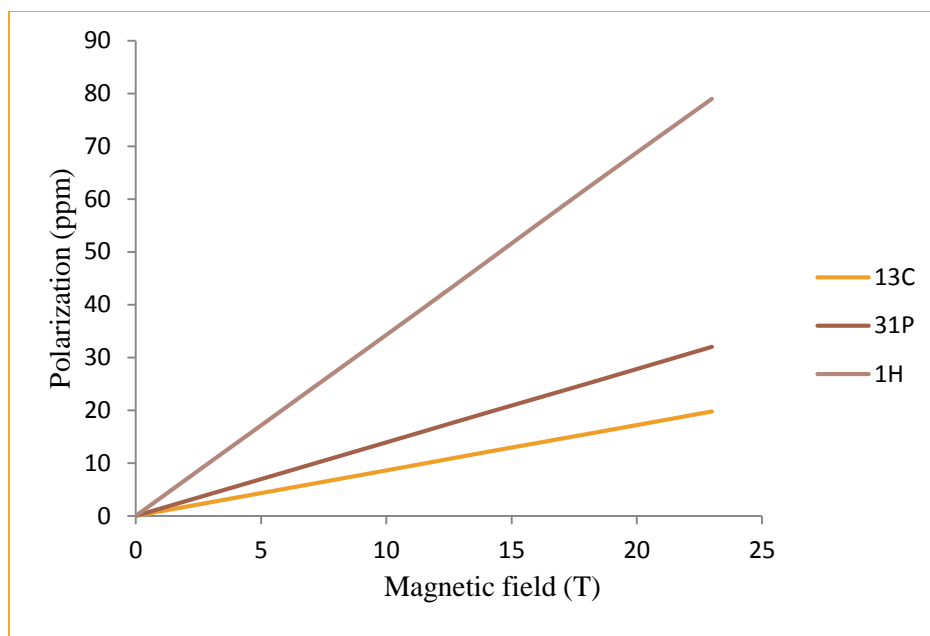
Figure 2.2 Plot of polarization of ^{1}H, ^{31}P and ^{13}C as a function of magnetic field at ambient temperature (298 K) as calculated by equation 2.9.

2.6 RF Excitations and NMR Signal Generation

The macroscopic effect of an external static magnetic field $\vec{B}_0$ is the generation of an observable bulk magnetization of the nuclei pointing in the direction of the external magnetic field, which is called the longitudinal component of the magnetization. Although, there is a transverse magnetization associated with each magnetic moment, the net transverse magnetization sums to zero at thermal equilibrium since each precessing moment has a random phase. The process through which phase coherence is developed among the randomly precessing spins is termed 'resonance'.

2.6.1 Larmor Condition

For the establishment of phase coherence among the randomly precessing spins, an external force in the form of an oscillating magnetic field $\vec{B}_1$ (t) is applied in addition to the static field $\vec{B}_0$.

$\vec{B}_1$ (t) field is short-lived and oscillates in the radio frequency range. It is synonymous with the RF pulse excitation of the system.

The classical argument of the resonance condition dictates that the field $\vec{B}_1$ (t) rotates in the same manner as the spins precessing around the static field $\vec{B}_0$. The quantum mechanical description of the resonance condition states that electromagnetic radiation of frequency ω_{rf} carries a certain amount of energy which is given by Planck's law:

$$E_{rf} = \hbar\omega_{rf} \qquad\qquad 2.10$$

To induce coherent transitions of the spins from one energy level to another, the energy of the RF excitation pulse must be equal to the energy difference between the energy levels.

$$\hbar\omega_{rf} = \Delta E = \hbar\gamma B_0 \qquad\qquad 2.11$$

$$\omega_{rf} = \omega_0 \qquad\qquad 2.12$$

2.6.2 Flip Angle

The effect of the on-resonance excitation $\vec{B}_1$ (t) field is a precession of the bulk magnetization vector about the axis along which $\vec{B}_1$ (t) points. In other words, this RF field causes the nutation of the spin ensemble. This precession is called the forced precession. The result of this forced precession is tipping of the longitudinal magnetization toward the transverse plane to create a measurable transverse component. The parameter that controls the amount of the longitudinal magnetization that is tipped into the transverse plane is called flip angle. Flip angle is the characteristic of the RF pulse that is applied for excitation. The flip angle describes the angle of

11

the magnetization vector relative to the static field direction, after it has been tipped by the applied RF pulse. In the case of a rectangular pulse, it is given by:

$$\theta = \gamma B_1 \tau_p \qquad\qquad 2.13$$

2.6.3 Free Induction Decay

The precession of the spin ensemble due to the application of the RF oscillation field (RF pulse excitation) induces an oscillating current in the receiver coils. In the spectrometer, this current is amplified, digitized and recorded. Free induction decay is the MR signal that arises due to the action of a single RF pulse on a nuclear spin system. 'Free' refers to the fact that this signal is generated due to the free precession of the bulk magnetization vector about the $\vec{B}_0$ field, 'induction' indicates that the signal is produced based on the Faraday's law of electromagnetic induction and 'decay' indicates that the amplitude of the signal dies out with time. FID signals are the most type of MR signals. The maximum amplitude if an FID signal depends on the flip angle of the RF pulse and the thermal equilibrium value of the bulk magnetization.

2.6.4 Fourier Transform

In a typical NMR experiment, the raw FID in time domain contains a multitude of information and is very hard to identify individual component waveforms. This raw FID is converted into frequency domain by Fourier transform. Fourier transform is a mathematical operation which converts time domain data into frequency domain. This way, if the MR signal has more than resonances, they can be viewed as separate signal peaks in the frequency domain, thereby simplifying analysis of NMR data.

2.7 Relaxation, T_1 and T_2

The laws of thermodynamics state that a spin system will eventually return to its thermal equilibrium state after the perturbation by an RF pulse provided the external RF field is removed and adequate time is given. This process is referred to as 'relaxation' and is characterized by the free precession of the bulk magnetization around the static field $\vec{B}_0$. The process involves recovery of the longitudinal magnetization M_z (longitudinal relaxation) and the destruction of the transverse magnetization M_{xy} (transverse relaxation).

The longitudinal relaxation is also called the spin-lattice relaxation and is dependent on a time constant T_1. Longitudinal relaxation occurs due to the exchange of energy between spins and the lattice. Spins experience resonant frequencies from other nearby spins and they flip randomly to return to their thermal equilibrium state thus releasing the extra absorbed energy to the lattice. T_1 characterizes the time after which the longitudinal magnetization has returned to 63% of its final value.

Transverse relaxation is also called the spin-spin relaxation and is faster or equal to the longitudinal relaxation [20]. This relaxation is responsible for destroying the phase coherence among precessing spins and hence the elimination of the transverse magnetization. The underlying mechanism for this relaxation is the interaction of the spins (spin-spin interaction) and the modification of their Larmor precession frequencies which leads to the phase incoherence. The time constant T_2 dictates the time at which the transverse magnetization has reached 63% of its initial value.

Both of these relaxation processes follow an exponential trend and can be given by Bloch equations.

$$\frac{dM_z}{dt} = -\frac{M_z - M_z^0}{T1} \qquad\qquad 2.14$$

$$\frac{dM_x}{dt} = \gamma\, M_y B_1 - \frac{M_x}{T2} \qquad\qquad 2.15$$

$$\frac{dM_y}{dt} - \gamma\, M_x = B_1 - \frac{M_y}{T2} \qquad\qquad 2.16$$

These equations are collectively called Bloch equations [21]. Felix Bloch was awarded a Nobel

Prize for his work in 1952.

Chapter 3: Theoretical Background of Dynamic Nuclear Polarization NMR

3.1 Lack of Sensitivity of NMR Experiments

Nuclear Magnetic resonance is one of the most important and widely used analytical and experimental techniques in chemistry, biology, materials sciences and life sciences. NMR is also the basis of the Magnetic Resonance Imaging which is a very important clinical imaging and diagnostic technique. Magnetic resonance imaging and spectroscopy (MRSI) is emerging as a very promising technique for in-vivo and in-vitro functional imaging. A few of the applications of the MRSI include brain imaging, imaging biomarkers and metabolic pathways for cancer research and therapy. Despite of its wide and crucial applications; however, NMR is limited by the inherent lack of sensitivity. This lack of sensitivity mainly stems from the low thermal equilibrium nuclear polarization of the sample. The low gyromagnetic ratios and low magnetic moments of the nuclei give rise to low nuclear polarizations P, a parameter which dictates the signal strength of the NMR signal.

As shown in Figure 2.2, the thermal equilibrium polarization for two of the most commonly used NMR nuclei, ^{1}H and ^{13}C, is less than even a 100 ppm throughout the usual range of magnetic fields applied in nuclear magnetic resonance experiments. Moreover, the increase in the polarization is linearly related to the increase in the magnetic field strengths and the overall sensitivity is proportionated with the magnetic field strength [3, 4]. However, the cost of NMR magnets tends to increase exponentially with the magnetic field strength. Also, present day superconducting technology is already at its upper limit in providing ultra-high magnetic fields [5]. Therefore, the

difficulty in the manufacturing of the magnets with ultra-high magnetic fields, economical constraints and technical limitations render this method of increasing the NMR sensitivity limited in its applicability.

Another simpler method to increase the signal to noise ratio of the NMR experiments is signal averaging. However, as the SNR is directly proportional to the $\sqrt{t}$, the SNR is increased at the cost of increased acquisition times for the experiments. Thus, increasing the sensitivity of NMR experiments by this method is not particularly the best method, especially in the functional imaging experiments where significantly lower acquisition times are required.

Other advances directed toward the sensitivity enhancement of NMR experiments involve probe design, cryo-probes and the use of micro-coils. All of these methods to increase the NMR sensitivity are basically the attempts of increasing the SNR. Nevertheless, the major impediment in the NMR sensitivity is the low polarization of the nuclei; population differences between the energy levels and hence, if targeted, provides the most margins for increase in sensitivity. The approaches used to achieve a larger polarization of the NMR sensitive nuclei are called 'hyperpolarization methods' and are by far the most promising techniques in enhancing the sensitivity of the MRSI experiments.

3.2 Hyperpolarization

As discussed above, increasing the sensitivity of the NMR experiments by increasing the magnetic field strengths or acquisition times are not the most desirable and feasible methods. Hence it is essential to employ other techniques to achieve a higher sensitivity. Hyperpolarization methods involve artificially increasing the nuclear spin polarization of the sample far beyond its thermal equilibrium polarization before the NMR experiment.

A number of hyperpolarization techniques are employed to increase the sensitivity of NMR and each of them have its benefits and drawbacks. While some techniques are easy to implement, others are more widespread owing to their suitability to certain applications. The main techniques to achieve hyperpolarization are 1) Optical pumping, 2) Para-Hydrogen induced polarization (PHIP) and 3) Dynamic Nuclear Polarization [6]. The technique most relevant to our purposes is Dynamic Nuclear Polarization and is discussed in detail.

3.3 Dynamic Nuclear Polarization

3.3.1 Introduction

Dynamic nuclear polarization (DNP) presents a technique to enhance the nuclear polarization of essentially any spin ½ nucleus. Methods have developed for DNP in solid and liquid states. The basic mechanism through which DNP operates is the transfer of very high electronic polarization of a paramagnetic species to the lower nuclear polarization of a NMR active diamagnetic species.

The concept of increasing the nuclear polarization in metals beyond the Boltzmann thermal equilibrium polarization was first introduced by Overhauser (Overhauser effect) [1]. This idea was based on the transfer of the polarization from electron to nuclei by saturating the electron transitions. He proposed that it was possible to enhance the population difference between the nuclear Zeeman levels by increasing the saturation of the conduction electron spin resonance (ESR) by a factor of several thousand thereby increasing the nuclear polarization in metals. This theory was soon tested and verified by Carver and Slitcher [2].

In the recent years, DNP has emerged as a significant technique to enhance the signal intensities and hence the NMR sensitivities. DNP can enhance the nuclear polarization by 10^3 - 10^4 which

can in turn reduce the acquisition times for the experiments by a factor of 10^6 - 10^8 as the SNR is directly proportional to the (number of averages)$^{1/2}$ [7].

The first application of dynamic nuclear polarization to enhance the signal to noise ratio by a factor of 10,000 in the liquid state NMR was demonstrated by Jan Henrick Ardenkjaer Larson and colleagues in 2003 [7]. All mechanisms of DNP depend on the RF irradiation as a means to transfer the electronic polarization to the nuclei. The RF irradiation frequency is close to the electronic (EPR) Larmor frequency at the magnetic field used for the experiment.

3.3.2 DNP vs Brute Force Methods

Due to the small gyromagnetic ratios and small magnetic moments of nuclei, the nuclear spin orientation or polarization by brute force methods necessitates a set of conditions that might be very hard to achieve, i.e., extremely low temperatures in milli-Kelvin range and very high magnetic fields of around 10 T. As shown in Figure 3.1, the spin polarization does indeed increase as a function of temperature when subjected to even moderate magnetic fields. However, obtaining polarization levels close to 100% requires temperatures in the milli-Kelvin range. Even if these conditions are achieved and maintained, the level of polarizations might still be very low as the Spin-lattice relaxation times are markedly long (hours to days) under these conditions. DNP is a technique to align the nuclear spins in a solid under a set of conditions that are easily achieved. The solid is doped with a small quantity of paramagnetic species i.e., free radical which are used to transfer the polarization to the nuclei of the substrate. Due to the large gyromagnetic ratio and magnetic moment of free electrons, the electronic spins are much more easily oriented (polarized) at the liquid He temperature and a magnetic field of 3 T. The process involves the irradiation of the sample with microwaves to transfer the higher polarization of electrons to nuclei.
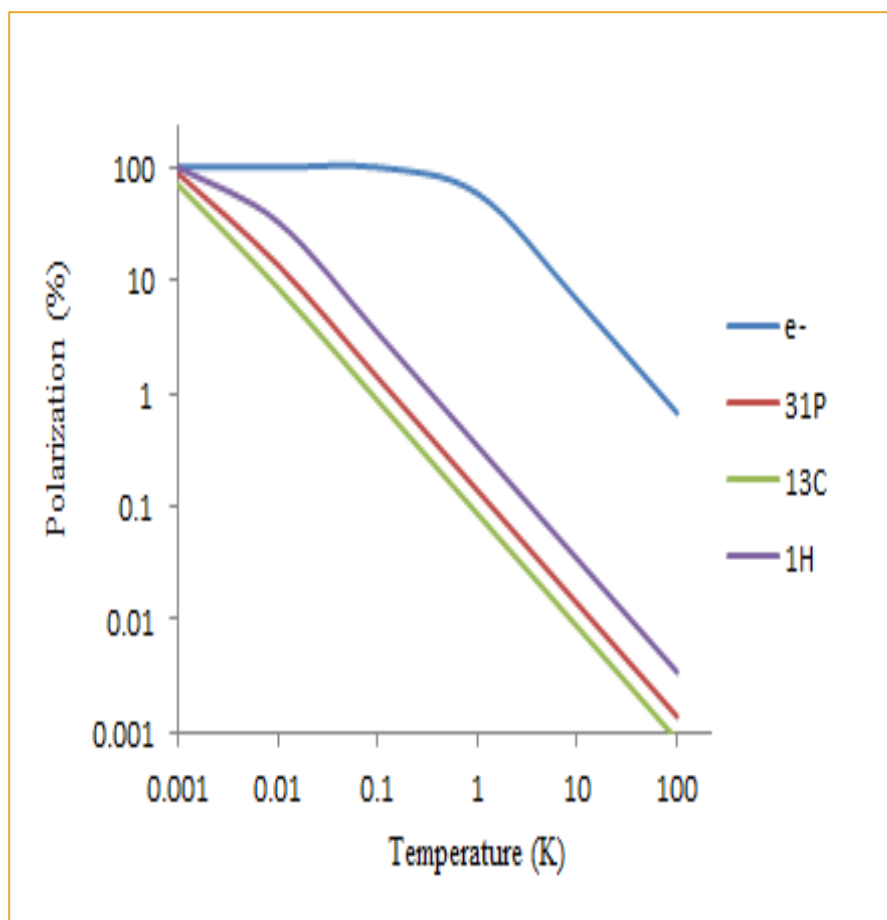
Figure 3.1 Polarization of ^1H, ^{13}C and e^- as a function of temperature with B_0 of 3.35 T as calculated from equation 2.9.

3.3.3 Overhauser Effect DNP

As discussed above, hyperpolarization in metals was proposed by Overhauser in 1953 [1]. Later, it was verified experimentally involving the studies of finely powdered metals and then later adapting the use of the dissolved alkali metals in liquid ammonia [2, 3]. Present day techniques involve the use of solutions containing a soluble stable free radical. The Overhauser effect relies on the stochastic interactions between the nuclear spins and electronic spins by saturating the electronic spin transitions in the presence of microwave irradiation. It is effective when the scalar or dipolar coupling is modulated by the relative motion between the electronic and nuclear spins.

19

If the timescale of the relative motion is $\leq 1/\omega_e$, where ω_e is the electronic Larmor frequency, then the probability of the transitions involving mutual electronic and nuclear spins is high and hence the transfer of the polarization. The above mentioned condition becomes harder to satisfy at higher magnetic fields as the ω_e becomes large. Thus, the efficiency of the OE DNP decreases at higher magnetic fields. Moreover, the reliance of the hyperpolarization on the stochastic interactions limits the application of Overhauser DNP to liquids and metals [14].

The Overhauser effect is limited by certain factors. For OE to be effective, it is necessary to use low frequencies and smaller samples. As the absorption of the microwave irradiation by the aqueous solutions cause heating of the sample, the efficiency of the polarization is reduced. For example, at a magnetic field strength of 0.35 T, the Larmor frequency of the electron is 9.8 GHz (X-band) and the suitable sample volume is 4 µl for one experiment [9]. The Overhauser DNP is, however, inadequate in its potential to reach maximum polarization levels due to the limiting factors of low magnetic fields and smaller sample volumes.

3.3.4 Dissolution DNP

Although it is extremely difficult to achieve a decent polarization in the nuclei with 'Brute force methods', it is possible to obtain a fairly high electronic spin polarization at relatively low temperatures (around 1.4K) owing to their high gyromagnetic ratios. Dissolution DNP involves hyperpolarizing the sample in a solid (frozen) form and then heating it to sufficiently high temperatures to dissolve it. In other words, the substrate/sample undergoes a freeze-thaw process. Contrary to the Overhauser DNP, Dissolution DNP is not limited to liquids or metals. It is technique which provides the capability of hyperpolarizing the non-paramagnetic species.

3.3.5 Experimental Considerations for Dissolution DNP

The polarization of the non-paramagnetic species involves the presence of a stable free radical for the purposes of transferring high electronic polarizations to the nuclei of the paramagnetic species. While it is possible to generate free radicals in the system through exposing the material to the ionizing radiation, the standard and most common practice is to add a paramagnetic species. A few of the most commonly used radicals are shown in the figure below. These radicals are used because of their desirable properties i.e., narrow EPR line widths, chemical stability and inertness under the experimental conditions.

The choice of the free radicals to be used with specific experiments further depends on certain experimental conditions, for example, the mechanism through which DNP proceeds, solubility of the free radical in the glassing agent/substrate mixture, etc.

Another important factor that affects the efficiency and the maximum achievable polarization levels is the spatial homogeneity of the sample. The electron spins need to be uniformly distributed in the sample. This condition is fulfilled by making sure that the sample is present in the amorphous form when it freezes. While some materials form a glassy solid upon freezing, other materials, especially aqueous samples, require the presence of a glassing agent to form an amorphous solid. The most common glassing agents used are glycerol, glycerol/water mixture, ethylene glycol, glucose, dimethyl sulfoxide, and methanol.

The sample is polarized at a magnetic field of 3.35 T and temperatures as low as 1.4 K. The microwave irradiation frequency is close to the electronic Larmor frequency. All of the above mentioned conditions play an important role in the maximum achievable polarization levels and need to be optimized for different substrates and free radicals.

As the polarization decays with the T_1 relaxation time and is available for about $5T_1$, it is imperative to transfer the sample to the NMR scanner as soon as possible after the dissolution for data acquisition.

3.3.6 Mechanisms of DNP

Following is a comprehensive and brief discussion of the different mechanisms through which DNP operates.

3.3.6.1 The Solid Effect DNP

The solid effect (SE) DNP mechanism is applicable to the solid state insulators. The DNP operates via the mechanism of solid effect in insulators when the concentration of the electronic spins is low and there is no significant interaction between the electronic spins [10]. When the characteristic EPR linewidth of the free radical is smaller than the nuclear Larmor frequency, the mode through the DNP operates is the SE. This process relies on single electron spin coupled with single nuclear spin. The basic mechanism of the SE through which the nuclear spins get polarized is the simultaneous flip-flop or flip-flip transitions of the electronic and nuclear spins. Irradiation frequency of electron Larmor frequency plus the nuclear Larmor frequency ($\omega_e + \omega_n$) induce the simultaneous electron nuclear 'flip-flop' spin transitions whereas the irradiation frequency of the electron Larmor frequency minus the nuclear Larmor frequency ($\omega_e - \omega_n$) induce the simultaneous electron nuclear 'flip-flip' spin transitions [19]. These simultaneous electron nuclear spin transitions are considered classically forbidden but become allowed upon the application of microwave irradiation. When the electron generates a finite magnetic field on the nucleus, the two become dipolar-coupled and this hyperfine coupling of the electron and nucleus gives rise to the small but persisting probability of the so called forbidden simultaneous electron nuclear spin

transitions [11]. Since the probability of these simultaneous spin transitions is low, the simultaneous spin transition process is slower than the relaxation of electron but is still faster than the nuclear T_1 relaxation. This is very crucial as the nuclear T_1 relaxation brings the nuclear spin polarization back to the thermal equilibrium state hence destroying the polarization. Figure 3.2 gives a pictorial representation of this mechanism.
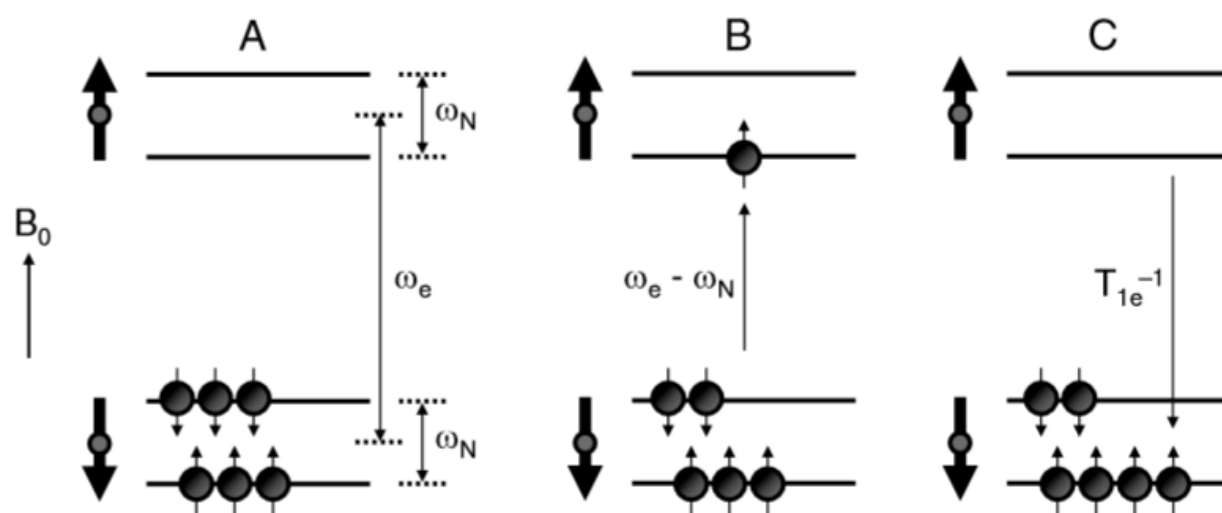
Figure 3.2 The mechanisms of solid effect. Nuclear spins are represented by small arrows whereas electron spins are represented by large arrows. (a) At thermal equilibrium, all the spins are approximately equally distributed over the two energy levels. (b) Upon the microwave irradiation at the frequency ω_e - ω_n, an electron-nuclear spin flip-flip transition occurs to a higher energy level. (c) Due to fast electron T_1 relaxation, the electron spin quickly returns to the lowest energy level while leaving the nuclear spin polarized. Continued microwave irradiation can quickly lead to large non-equilibrium nuclear spin polarization. (Adapted from de Graaf with permission).

3.3.6.2 Thermal Mixing DNP

When the EPR linewidth of the free radical is equal to or larger than the nuclear Larmor frequency and the concentrations of the electron spins is high, DNP operates through a different mechanism which is known as thermal mixing [10]. In thermal mixing, unlike the solid effect, the electron-electron interactions are much stronger than the electron-nuclear interactions and the process relies on an ensemble of electron spins rather than a single electron spin for electron nuclear spin

transitions. Thermal mixing can be viewed as a two-step process. First, the microwave irradiation close to the electron Larmor frequency drives an electron-electron flip-flop spin transition. And in the next step, electron-electron cross relaxation between spins in the EPR line with an energy difference of $\omega_n = (\omega_{e1} - \omega_{e2})$ induces a nuclear spin flip transition leading to a net nuclear polarization buildup in a 3-spin energy conserving mechanism. Figure 3.3 shows this mechanism.

Microwave irradiation

| Electron spin | Electron spin | Nuclear spin | | Electron spin flip | Electron spin flop | Nuclear spin flip |
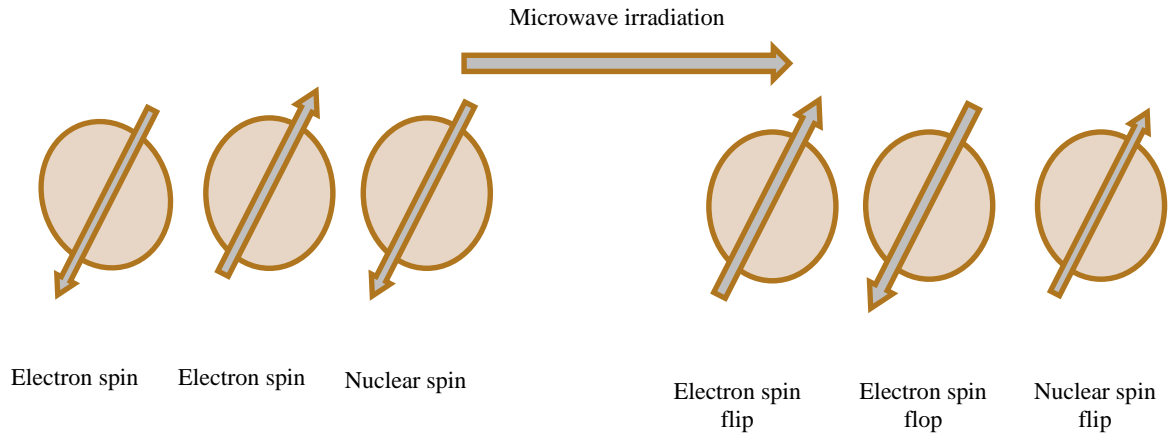
Figure 3.3 3-spin process of thermal mixing

One other way that the thermal mixing mechanism can be viewed is the thermal coupling of the electron dipole system and the nuclear Zeeman system. Microwave irradiation close to the electron Larmor frequency reduces the spin temperature of the electron dipole system which in turn brings down the spin temperature of the nuclear Zeeman system as both of them are thermally coupled [12,13].This thermal coupling leads to high nuclear spin polarization. As the thermal mixing relies on the allowed transitions, it is more efficient as compared to the solid effect. Figure 3.4 illustrates this mechanism.
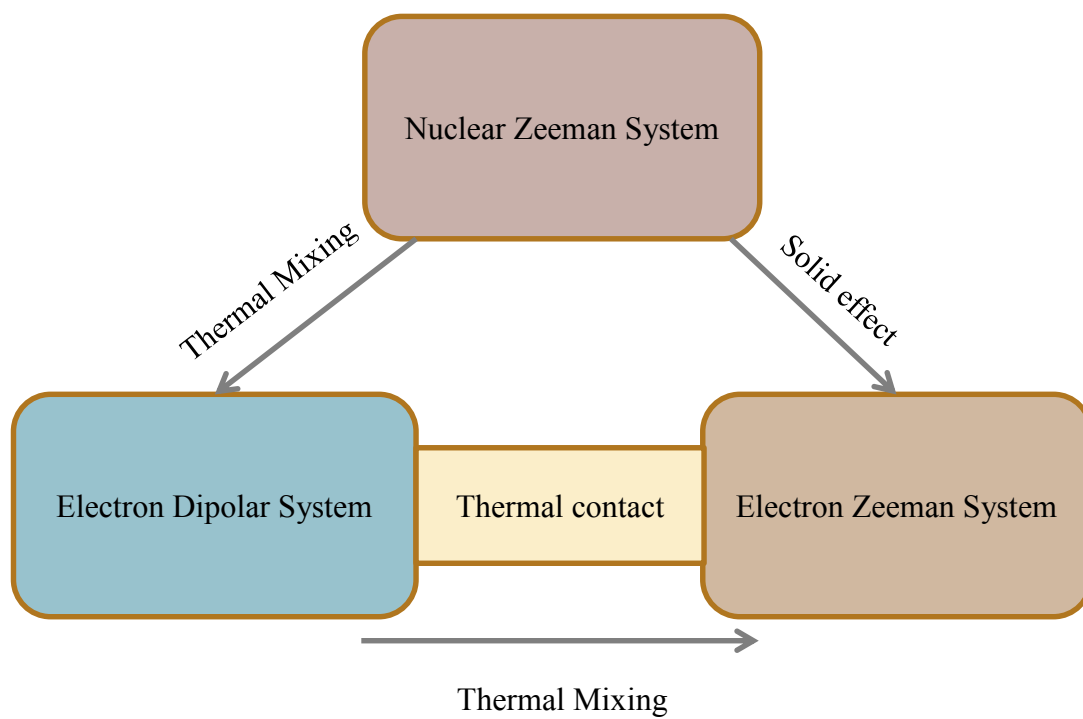
Figure 3.4 Thermodynamic view of the DNP by thermal mixing. The electron dipolar system is in thermal contact with the nuclear Zeeman system.

Chapter 4: Materials and Methods

4.1 Sample Preparation

All samples were prepared by mixing the neat solvent DMMP with a glassing agent. The glassing agent used for the experiment was the mixture of glycerol and water in the volume ratio of 1:1. The final concentration of the sample contained DMMP and the glassing matrix in the volume ratio of 1:1. Two radicals, a nitroxyl radical (2,2,6,6-Tetramethyl-piperidin-1-yl)oxyl TEMPO and a trityl radical OX063 were used. The radicals were dissolved in the DMMP and glassing matrix mixtures such that a final concentration of 40mM for the radical TEMPO and of 15mM for the radical OX063 was obtained. All the samples were tested for glass formation by immersing in the liquid nitrogen.

4.2 Different Combinations of Sample Preparation and Experimental Conditions

Polarization buildup with the radical OX063 was monitored for 3 different sets of glassing agent and microwave frequency conditions.

1) Glycerol and D_2O mixture, D_2O used as the dissolution solvent and sample polarized at the microwave irradiation frequency of 94.080GHz.

2) Glycerol and dI H_2O mixture, dI H_2O used as the dissolution solvent and sample polarized at the microwave irradiation frequency of 94.080GHz.

3) Glycerol and D_2O mixture, D_2O used as the dissolution solvent and sample polarized at the microwave irradiation frequency of 94.066 GHz.

Polarization buildup with the radical TEMPO was monitored for 2 different sets of glassing agent and microwave frequency conditions:

1) Glycerol/ D_2O mixture, D_2O was used as the dissolution solvent and sample polarized at the microwave irradiation frequency of 94.100 GHz.

2) Glycerol and D_2O mixture, D_2O used as the dissolution solvent and sample polarized at the microwave irradiation frequency of 94.174 GHz.

Following is the table summarizing all the above mentioned conditions.

Table 4.1 Summary of different sample preparation and experimental conditions

Radical	Glassing Agent	Dissolution Solvent	Irradiation Frequency (GHz)
OX063	Glycerol/D_2O	D_2O	94.080
OX063	Glycerol/D_2O	D_2O	94.066
Ox063	Glycerol/dI H_2O	dI H_2O	94.080
TEMPO	Glycerol/D_2O	D_2O	94.100
TEMPO	Glycerol/D_2O	D_2O	94.174

4.3 Polarization

4.3.1 The Hypersense DNP Polarizer

The Hypersense DNP polarizer is a commercial instrument manufactured and marketed by Oxoford Instruments [15]. The instrument is based on the work done by Jan Henrick Ardenkjaer Larson and M. Golman [7]. The Hypersense polarizer consists of a supercooled, superconducting magnet of with a magnetic field strength of 3.35 T and a dissolution system to dissolve the frozen sample into a liquid after the polarization. After the sample has been prepared with a glassing mixture and a doping agent, it is placed into a sample cup made from Poly(fluorenylene ethynylene) (PFE). The glassing mixture added to the sample makes sure that the sample forms an amorphous solid upon freezing. This condition is very crucial to satisfy as it avoids the aggregation of the sample constituents in the mixture and spreads the electron spins uniformly throughout the sample for an effective polarization transfer. The sample cup can hold up to 200 µl of the sample. A volume of 180 µl was used for my experiments unless otherwise stated. After the system has been prompted and prepared for the sample cup insertion, the cup is inserted via a special insertion stick. The insertion stick is vented, about 1 meter long and has a special release mechanism at the end to release the sample cup inside the cryostat. After the sample cup has been lowered and inserted into the cryostat, it sits in the surrounding bath of liquid helium. The cryostat has a constant supply of liquid helium through a cylinder that is permanently attached to it. The liquid helium allows for the temperature around the cup to be driven down to 1.2-1.4 K via the Joule-Kelvin effect. The time it takes for the system to cool down completely after the sample cup insertion is usually 3-5 minutes. After the insertion of the sample, the system is setup to provide microwave irradiation frequency and polarize the sample. The optimum frequency for the experiment is calibrated through another experiment known as the DNP microwave sweep

experiment, which will be discussed below. The microwave source power typically used is 100 mW. The time for complete and maximum polarization depends upon the sample under consideration. It is typically 60-90 minutes for ^{13}C compounds, a couple of hours for Si, and almost 3 hours for ^{31}P compounds. After the sample has been completely polarized, the system is prepared for the dissolution process. A syringe of 1.5-4mL, depending on the amount of the sample being hyperpolarized, is required to inject the dissolution solvent in the solvent heater. For my experiments, around 4 mL of the dissolution solvent was used for each dissolution process. The hyperpolarized sample dissolved in the solvent is delivered through a 1 mm lumen high density polyethylene (HDPE) tube by a stream of heated, high pressurized solvent. The dissolution process takes about 2 minutes, it is the time taken by the solvent to heat and the pressure to reach 10 bar in the pressure vessel which is called "the bomb". After the dissolution process, the hyperpolarized sample and solvent mixture was collected in a 4 mL clear, polymer container and manually transferred and inserted into a 7 T NMR spectrometer for data acquisition. The time taken for manual transfer and insertion is approximately about 12-15 seconds. During the transfer and insertion process, the sample does not pass through a zero magnetic field at any point. This is very crucial for the retention of the polarization.

4.3.2 DNP Microwave Irradiation Frequency Sweep and Calibration

The HyperSense instrument does not have the capability of monitoring polarization buildup for materials other than ^{13}C compounds. The microwave irradiation frequency is absolutely a very critical parameter that affects the maximum polarization buildup. For this series of experiments, we collaborated with William Mander from Oxford Instruments who assisted with the experiments and provided us with a solid state probe that can be tuned and matched to ^{31}P resonance frequency at 3.35 T (≈57.87 MHz) and inserted into the HyperSense cryostat. The sample cup containing

DMMP sample doped with the radical was inserted at the end of the solid state probe and placed into the HyperSense cryostat. A tuning and matching box connected to the other end of the tube was used to tune and match the probe to the right frequency. The probe was connected to the the Agilent ASR 310 scanner (Agilent Technologies, Santa Clara, CA) through the preamplifier low RF frequency channel used for ^{31}P, and scanner was used to pulse and acquire spectra. The computer attached to the NMR scanner was used to monitor the frequency sweep using the proprietary software VnmrJ 4.0. As the microwave irradiation and the monitoring were being done on two different instruments, several precautionary measures were taken and tests were done to ensure that the two events were completely synchronous. Microwave frequency was calibrated for both the radicals TEMPO and OX063. A microwave frequency sweep range with fixed step sizes / intervals was programmed into the HyperSense. The microwave source was turned on and the sample was allowed to polarize for about 2 minutes before hitting it with a $\pi/2$ pulse to acquire the signal. The $\pi/2$ pulse was applied to obtain the maximum signal strength. After the first $\pi/2$ pulse, a train of several more $\pi/2$ pulses was applied to kill any residual polarization buildup and the hypersense microwave source moved to the next frequency in the range for the sample to polarize at that frequency. The cycle was repeated for each frequency point in the entire range. The dead time encountered due to time it takes for the hypersense to move to the next frequency point in the range was carefully calculated and filled up by the corresponding number of $\pi/2$ pulses at fixed intervals so as to keep the polarization buildup time a constant of 2 minutes for each point of frequency in the range. Figure 4.1 shows the solid state probe used for the frequency sweep and calibration.

Figure 4.1 Solid state probe used for the ^{31}P microwave sweep and calibration with OX063 and TEMPO.

4.4 NMR Spectroscopy and 2D Multi-Slice Imaging

4.4.1 NMR Data Acquisition and Analysis for Spectroscopy and Hyperpolarization Calculations

DNP enhanced NMR experiments differ in their techniques and approach from the standard NMR experiments. In the standard, one dimensional spectroscopic experiment, a repetition time (TR) of $3T_1$-$5T_1$ is used between the subsequent scans to allow the polarization to return to the thermal equilibrium. Also a higher flip angle, normally a 90 degree RF pulse is used to tip the maximum amount of longitudinal magnetization in the transverse plane to get a maximum signal. For the DNP NMR experiments, however these two experimental conditions are not desirable because they result in the loss of hyperpolarization which is available for the time of almost $5T_1$ and it is essential to make use of all of the available hyperpolarization before it is gone either by longer repetition/delay times or destroyed by higher flip angles. Higher flip angles destroy the hyperpolarization as the relaxation in the hyperpolarized samples does not recover the hyperpolarized state but instead relaxes to the thermal equilibrium polarization.

To counter these problems, two different approaches are used in the standard one dimensional DNP spectroscopy experiments. These approaches make use of very small repetition times (TR), on the order of milliseconds and enable the experimenter to acquire multiple scans from a single hyperpolarized sample. Moreover, very small flip angles are used in both of the schemes to make sure that only a fraction of the total available hyperpolarization/longitudinal magnetization is used for each scan. In the first scheme, a train of RF pulses with a constant small flip angle is applied with a repetition time of some milliseconds. Each small flip angle RF pulse makes use of only a portion of the total available longitudinal magnetization. Since the hyperpolarization decays with T_1, each subsequent scan is less intense than the preceding one. This scheme has been used to measure T_1 with the hyperpolarized samples [16]. Following an RF pulse with a flip angle θ and an initial magnetization M_{DNP}, the remaining longitudinal magnetization is given by:

$$M_z = M_{DNP} \cdot \cos \theta \qquad\qquad\qquad 4.1$$

whereas the observable transverse magnetization is given by:

$$M_{xy} = M_{DNP} \cdot \sin \theta \qquad\qquad\qquad 4.2$$

Hence, a constant flip angle pulse sequence generates a steadily decreasing signal profile with each subsequent scan. Although it is possible to obtain an approximately uniform intensity weighted signal profile by using very small flip angles, it would be done at the cost of a major portion of the longitudinal magnetization/hyperpolarization remaining unused.

The other scheme involves using incremental flip angles for each subsequent scan to allow for the transverse magnetization stay constant and generate a uniform intensity signal profile. The highest and last RF pulse in this variable flip angle scheme is normally a 90 degree pulse. With this scheme, it is possible to use all or most of the available longitudinal magnetization while generating spectra

with uniform intensity. The flip angle θ for a kth scan, when the effects of T_1 relaxation are ignored, is given by [17, 18]:

$$\theta_k = arcsin\sqrt{1/(n + 1 - k)} \qquad\qquad 4.3$$

whereas the flip angle θ for a kth scan, when the effects of T_1 relaxation are taken into account, is given by [18]:

$$\theta_k = arcsin\sqrt{(1 - \beta\wedge 2)/(\beta\wedge(2(kn)) - \beta\wedge 2)} \qquad\qquad 4.4$$

where $\beta = e^{-TR/T1}$ and TR is the repetition time or the time between each scan.

In my experiments, the first scheme was employed for the measurement of T_1 times and the first scan of the hyperpolarized sample obtained through this method was also used for the calculations of polarization buildup and signal enhancements. Thermal equilibrium scans were also obtained for each experiment and used for the polarization buildup and signal enhancement calculations. Thermal equilibrium scans were acquired using 64 averages and a repetition time of 60 s ($\approx 5T_1$) was used to ensure the longitudinal magnetization recovery before each subsequent scan and a better SNR. The intensities of the thermal equilibrium scans were divided by 64 to compare the signal enhancements and to calculate the polarization buildup since signal intensities go up with the number of averages.

All data were acquired using a 7-T horizontal magnet (ASR 310, Agilent Technologies, Inc.) which is equipped with nested 205/120/HDS gradient insert and a bore size of 310 mm. A 33 mm double resonance ^{1}H,^{31}P RF coil (Doty Scientific, Inc., Columbia, SC) was used for the acquisition of all the spectroscopic and imaging data.

All the data were analyzed and calculations for polarization buildup and signal enhancements were done using in-house MATLAB™ routines.

4.4.2 Gradient Echo Multi-Slice (GEMS) Imaging

GEMS make use of the gradient echos. An echo is a NMR signal which differs from the free induction decay (FID) signal in the sense that it has 'two sides'. One side of the echo is generated from the refocussing phase (spins getting coherence) of the transverse magnetization and the other side is generated from the dephasing period (spins getting out of coherence). Such a two sided signal is required for the full coverage of the k space. A gradient echo is often used in combination with a small flip angle excitation for fast imaging. In a gradient echo pulse sequence a slice selective RF excitation pulse is applied to the object being imaged. The RF excitation pulse is followed by a phase encoding gradient and a dephasing frequency encoding gradient. The phase encoding gradient and the frequency gradient are applied at the same time to make sure that the spins are in phase at the middle of the acquisition period. After that another frequency encoding gradient, which is negative in sign than the first frequency encoding gradient, is applied to rephrase the spins which were dephased from the first frequency encoding gradient. The application of these two reversed frequency encoding gradients produces an echo. The sequence is repeated every TR (repetition time) seconds. The time from the start of the RF pulse to the center of the signal acquisition is called echo time (TE). TE is the time when the maximum signal is obtained. A timing diagram of the gradient echo sequence is shown in Figure 4.2. Gradient echo imaging sequences are advantageous to use with hyperpolarized substrates as they use a lower flip angle and fast repetition times, the two factors which are essential in conserving the available hyperpolarization.

In my experiment a gems sequence with TR of 7ms and TE of 2.32ms with a flip angle of 10 degrees was used. The experimental setup queue consisted of an alternating single pulse and a

gems sequences to obtain a spectrum followed by an image. The experiment showed the decaying hyperpolarized signal in the spectrum and decaying hyperpolarized image.
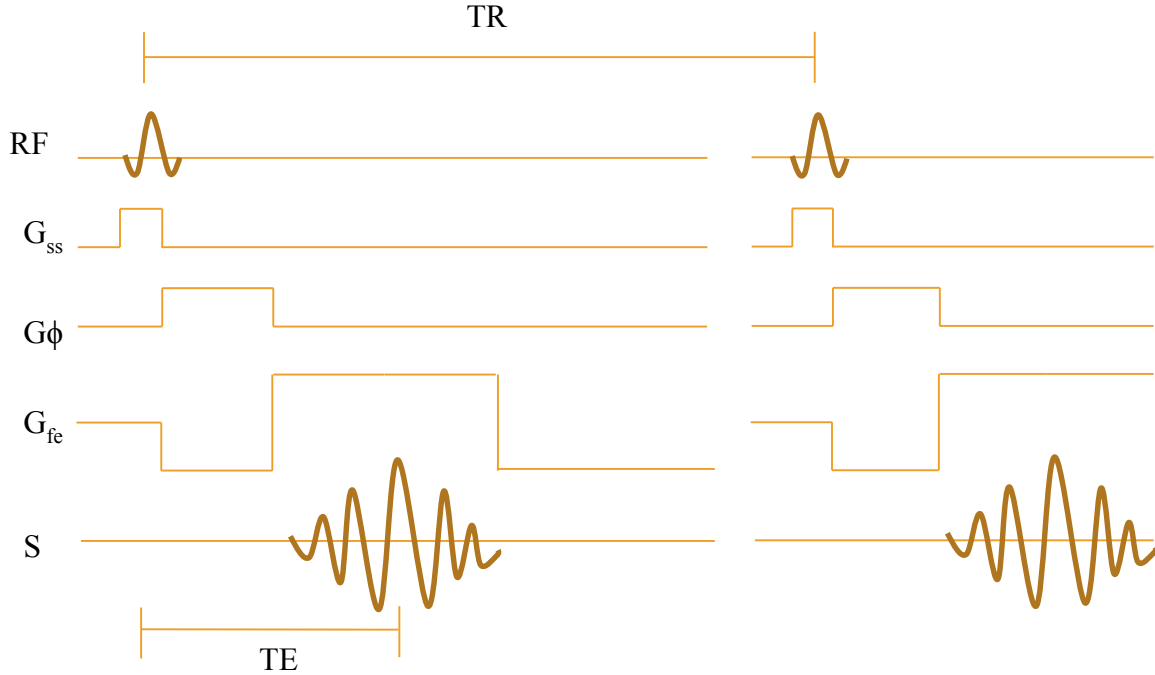
Figure 4.2 Pulse-sequence timing diagram of gradient echo multi-slice sequence (GEMS).

4.4.2.1 GEMS Imaging with Hyperpolarized DMMP Phantom

In this experiment, a GEMS sequence with TR of 7 ms and TE of 2.32 ms with a flip angle of 10 degrees was used. The matrix size of the acquired images was 32×64 matrix. A receiver bandwidth of 50 KHz bandwidth, FOV = 4cm(axial) × 4cm(transverse) and 1 slice of 3 mm thickness was used to acquire the images. The experiment consisted of two component sequences: alternating single pulse and GEMS to obtain a spectrum followed by an image. The experiment showed the decaying hyperpolarized signal in the spectrum and decaying hyperpolarized image.

4.5 In-vivo Imaging Protocol with Hyperpolarized DMMP

A nude male mouse, weighing approximately 27g was injected with hyperpolarized DMMP and imaged. Prior to the experiment, the mouse was anaesthetized using 3% isoflurane and housed in a mouse cradle. Following the anesthesia, the level of isoflurane was reduced to 2%. Respiratory function and the heart rate of the mouse were constantly monitored throughout the experiment using the SAII system (Small Animal Instruments, Inc.). The temperature control was achieved by a gas unit which was set to maintain a body temperature of $37\pm1°C$. A catheter was inserted, with a plastic tube of approximately 1 m length, in the tail vein of the animal for the administration of hyperpolarized DMMP. 100 µL of saline solution was placed in the catheter to compensate for the dead volume with the injection of the hyperpolarized DMMP. The animal was placed in an MR compatible insertion device to immobilize it inside the scanner in the prone position with head inserted first in the scanner and the anesthesia was maintained by delivering the isoflurane through a nose cone. The sample was prepared and dissolved in the manner described below and injected into the tail vein catheter after the dissolution. A total of 250 µL of the dissolved sample, containing 7.8 µL of hyperpolarized DMMP was administered for this experiment. A total of 100 µl of the sample which contained DMMP, radical OX063 and glassing mixture of D_2O/glycerol was hyperpolarized at the microwave frequency of 94.080 GHz for about 3 hours. Following the polarization, the sample was dissolved with 1.5 mL of the D_2O based solution containing 100mg/liter of disodium EDTA, 3.2g/liter of NaOH, 5.96g/liter of Trizma preset crystals pH 7.6 and 2.9g/liter of NaCL and transferred to a syringe for injection. The time from the dissolution of the sample until the injection in the mouse was about 20 seconds. All the animal experimental procedures including the injection of hyperpolarized DMMP were approved by IACUC.

The MRSI experiment was designed with a GEMS sequence alternating with a single pulse sequence to obtain spectra and images of hyperpolarized DMMP in-vivo. A GEMS sequence with a TR of 4 ms and TE of 2.02 ms with a flip angle of 20 degrees was used. The matrix size of the acquired images was 32×32, receiver bandwidth of 50 KHz, FOV = 8cm(axial) × 4cm(transverse) and 1 slice of 30 mm thickness was used to acquire the images of hyperpolarized DMMP. The spectra of the hyperpolarized DMMP were acquired using a single pulse sequence with a flip angle of 15 degrees and TR of 50 ms.

The images of the hyperpolarized DMMP were registered with the ^{1}H coronal section anatomical images, which were also acquired with the GEMS sequence. The imaging parameters were TR/TE = 90 ms/4.11 ms, 20 degrees flip angle, FOV = 8cm(axial) × 4cm(transverse), 1.50 mm slice thickness and data matrix= 128×128.

Chapter 5: Results and Discussions

5.1 Microwave Sweep Results

5.1.1 Microwave Sweep for Radical TEMPO

The microwave sweep for the radical TEMPO was done for two microwave frequency ranges. The first sweep was one with the range 94.050 GHz-94.25 GHz with a step size of 10 MHz. The results of this sweep indicated that the maximum enhancement was obtained around 94.100 GHz. Then the range for the second microwave sweep was shifted a little bit (94.230 GHz-94.27 GHz) and the experiment was performed with a step size of 17 MHz to confirm the optimum frequency. The results of the latter sweep also indicated the frequency 94.100 GHz to be the optimum frequency for the maximum enhancement. The following figures show these results.
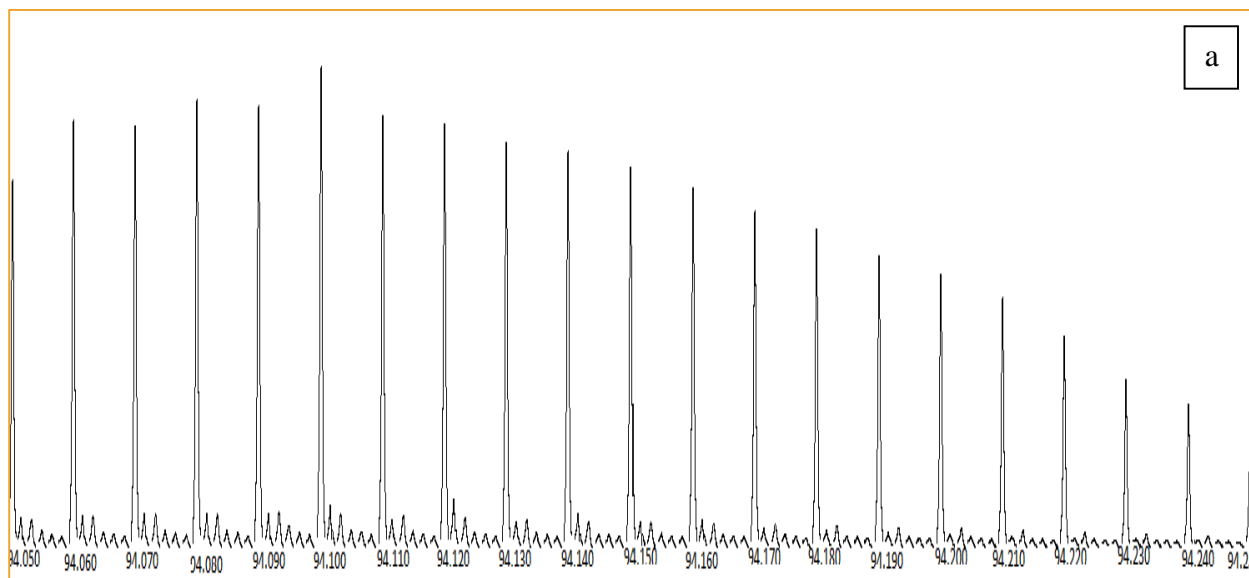

Figure 5.1 Microwave sweep for TEMPO. The maximum signal acquired at 94.100 GHz (a) the microwave sweep for the range 94.050 GHz – 94.250 GHz. (b) The microwave sweep for the range 94.930 GHz – 94.270 GHz
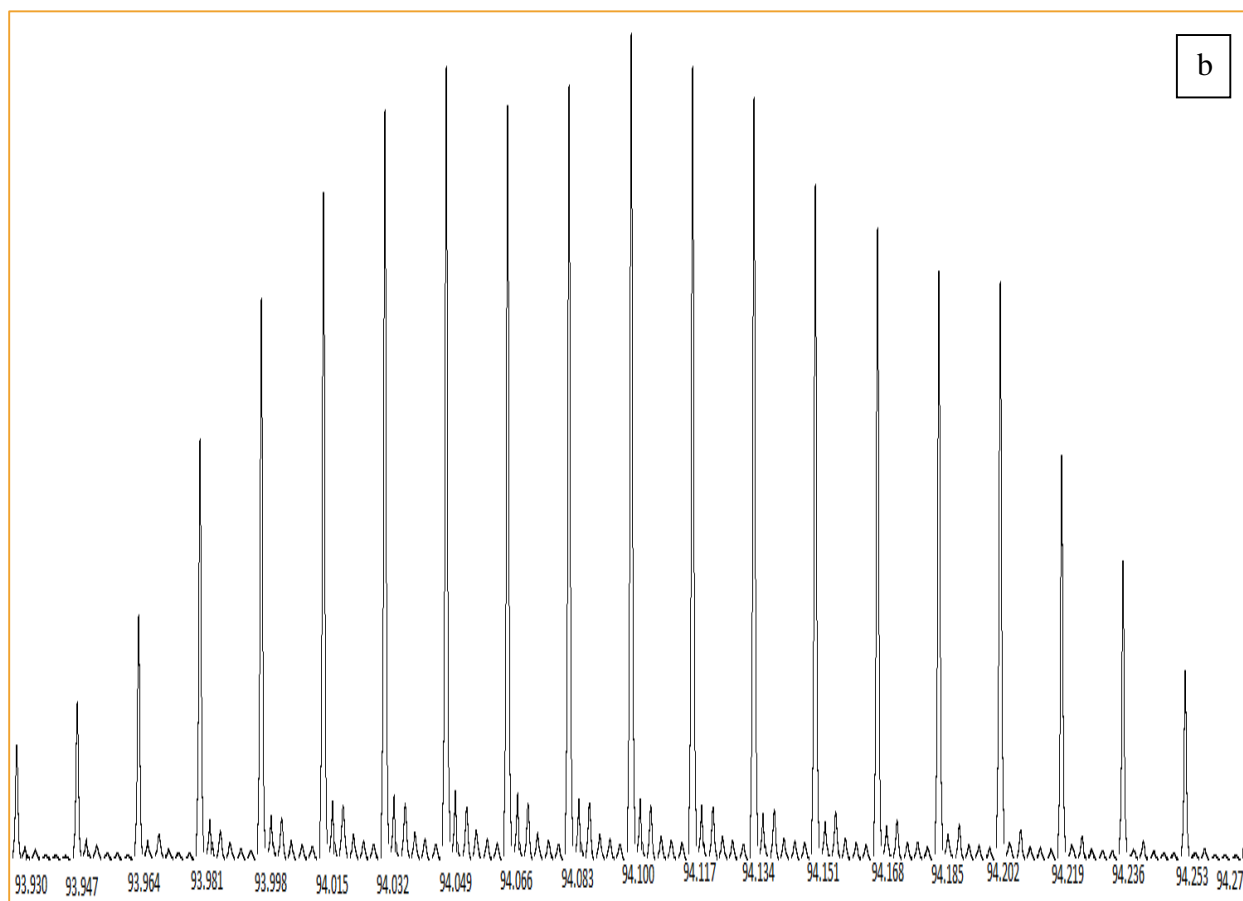
93.930 93.947 93.964 93.981 93.998 94.015 94.032 94.049 94.066 94.083 94.100 94.117 94.134 94.151 94.168 94.185 94.202 94.219 94.236 94.253 94.27

Figure 5.1 (Continued)

5.1.2 Microwave Sweep for Radical OX063

The microwave frequency sweep for the radical OX063 was done for the range 94.020GHz-94.220GHz. The results are shown in figure 5.3. The optimum frequency for the maximum enhancement was found to be 94.080GHZ. First peak is the positive polarization peak whereas the second peak is the negative polarization peak. Due to the narrower line width of the radical OX063, both of these peaks could be seen for the tuning range of the apparatus. The negative polarization peak values appear to be positive because the data are represented in the absolute peak

values. The following figure shows the range and the optimum frequency for the largest enhancement for DMMP with the radical OX063.
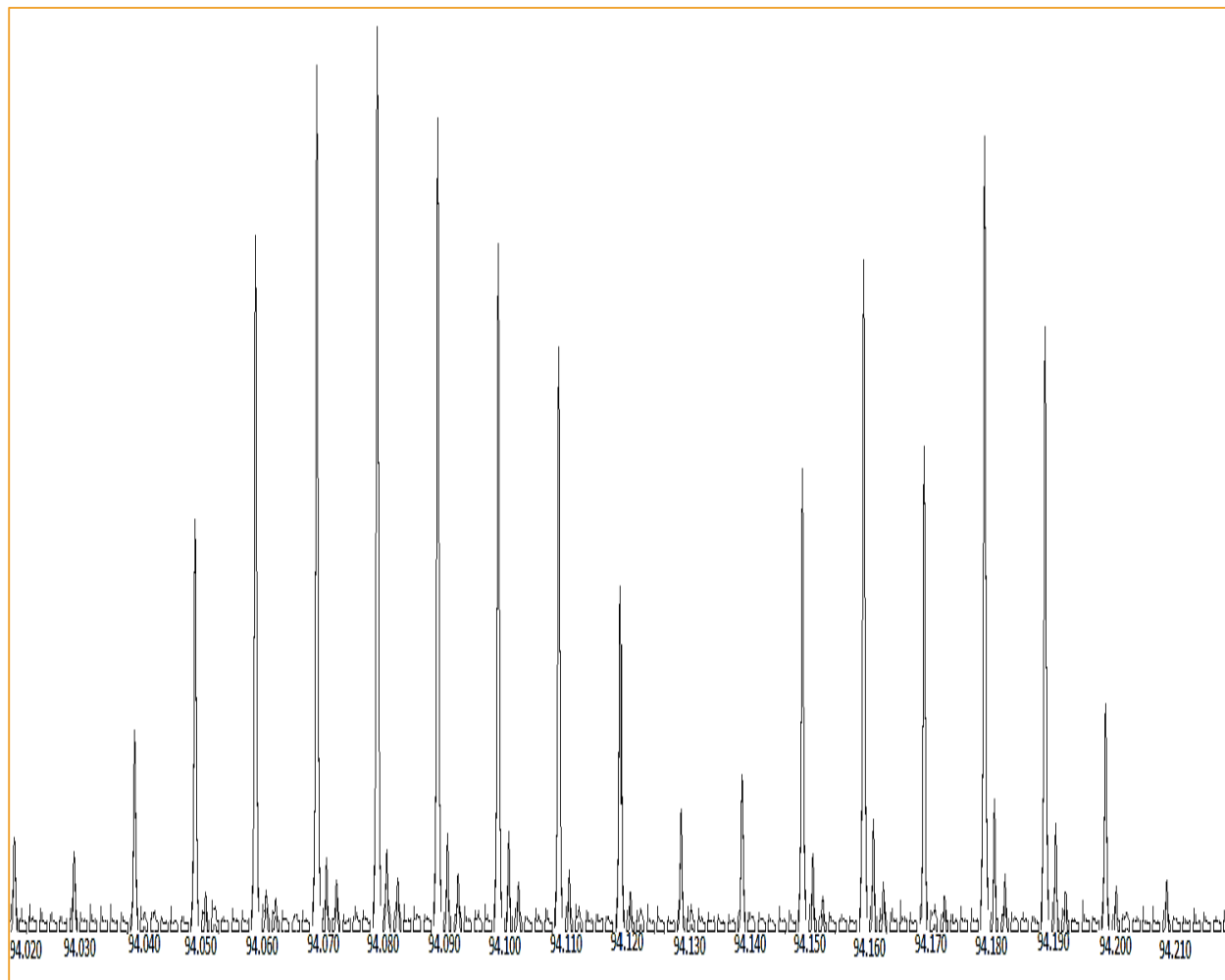
Figure 5.2 Microwave sweep for OX063

5.2 Polarization Buildup Time for DMMP with Radical OX063

The polarization buildup time for DMMP with the radical OX063 was monitored at the microwave frequency of 94.080 GHz as shown in figure 5.3. A 5 degrees RF pulse was used to acquire the hyperpolarized spectra every 5 seconds. The smaller flip angle was used to conserve the polarization buildup. The following figure shows that that optimum polarization buildup time for

DMMP with the radical OX063 at the microwave frequency is almost 3 hours. After 3 hours, the maximum intensity of the peaks was obtained.
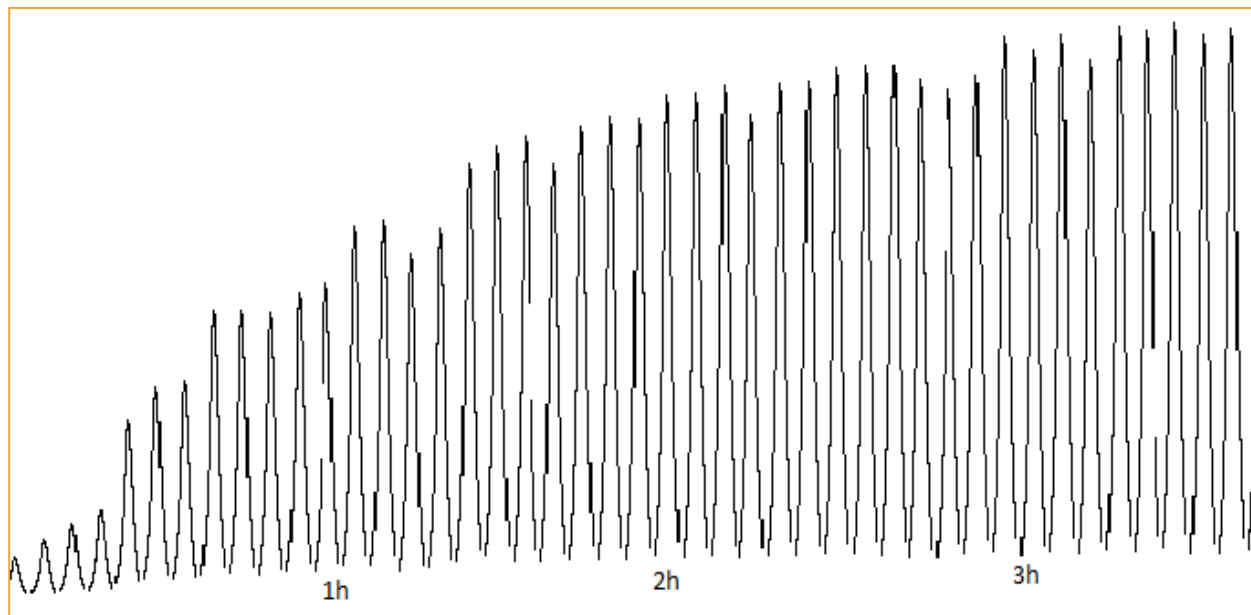

Figure 5.3 Polarization buildup time for DMMP with OX063

5.3 Polarization Buildup and Signal Enhancements

5.3.1 Polarization Enhancements with Radical OX063

5.3.1.1 Case 1: Glassing Agent: Glycerol/ D_2O Mixture and Microwave Irradiation Frequency: 94.066 GHz

The NMR data were collected for these calculations and results according to the scheme mentioned in section 4.4.1. Polarization of DMMP with glycerol and D_2O mixture as the glassing agent and at the microwave frequency of 94.066 GHz resulted in a 1939 fold signal enhancement and a corresponding polarization buildup of 1.8%. Figure 5.5 shows the intensity (arbitrary units) of the highest hyperpolarized spectrum obtained with a single RF pulse of 25 degrees. Figure 5.6 gives a comparison of the logarithmic intensity enhancement of the hyperpolarized signal as compared to

41

the thermal equilibrium signal. Figure 5.4 shows the T_1 weighted decay of the hyperpolarization

signal with time.

Table 5.1 Polarization enhancement with OX063 - case 1 results

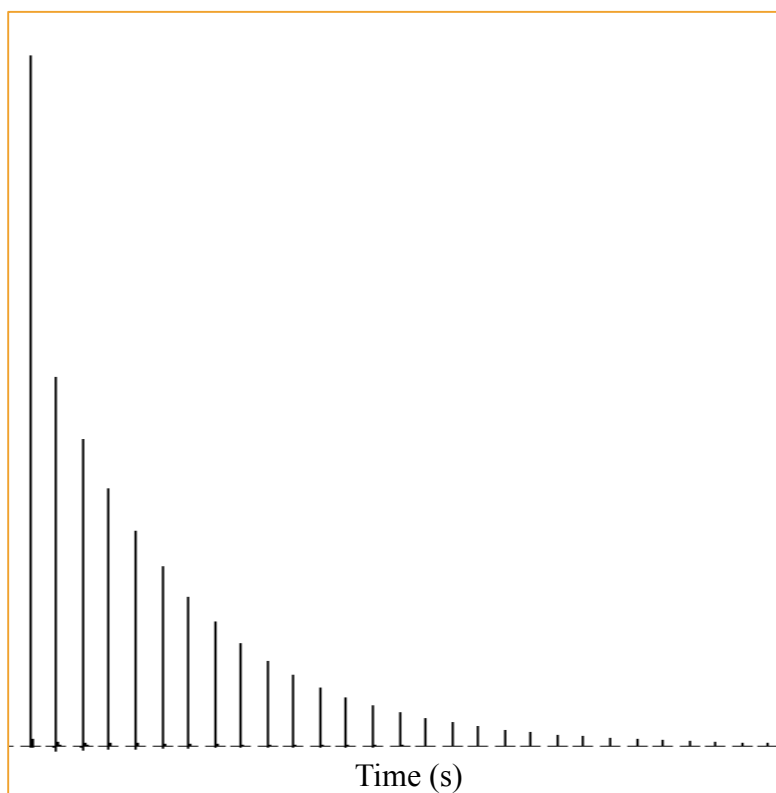| Enhancement	Percent Polarization buildup	Polarization of hyperpolarized signal	Polarization of thermal equilibrium signal
1939 fold	1.8%	0.018	9.34e-06

Time (s)

Figure 5.4 T_1 weighted decay of the hyperpolarized signal obtained with OX063-case1. Each signal was acquired using a single scan with a repetition time of 2 seconds. The hyperpolarized signal is available for almost 40 seconds after the insertion of the sample in the scanner.
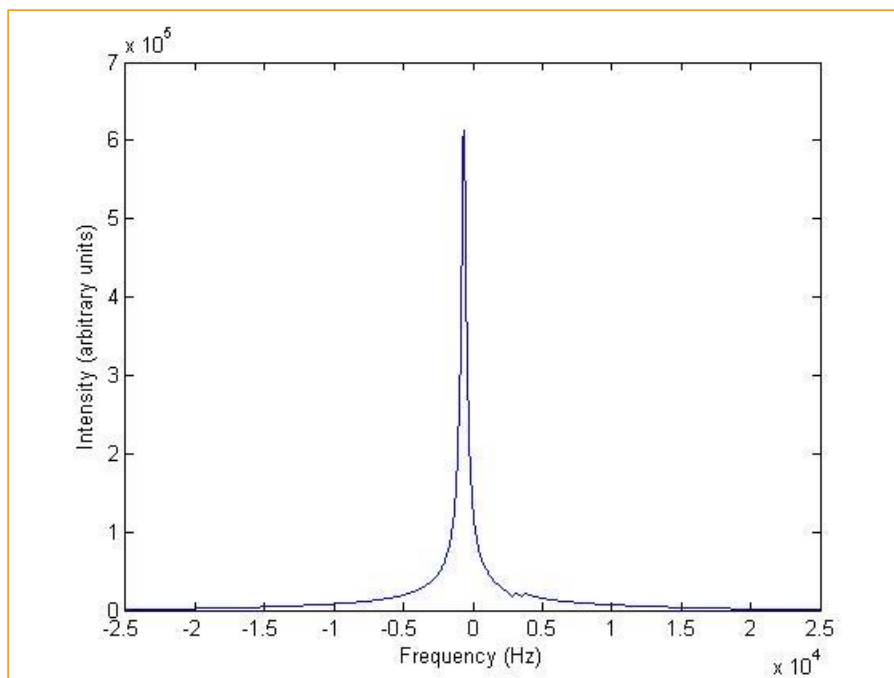
42

Figure 5.5 Highest hyperpolarized spectrum obtained with OX063-case 1. The spectrum was obtained with a single RF pulse of 25 degrees
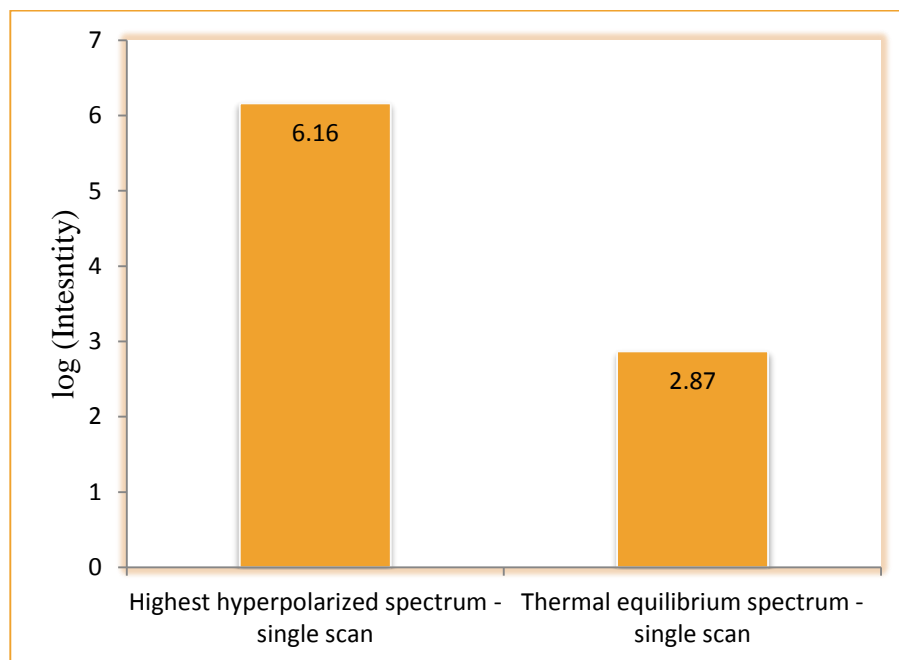

Figure 5.6 Intensity comparison between the highest hyperpolarized spectrum and thermal equilibrium spectrum obtained with OX063-case 1. The Intensities are represented on a logarithmic scale.

5.3.1.2 Case 2: Glassing Agent: Glycerol/ D_2O Mixture and Microwave Irradiation

Frequency: 94.080 GHz

The NMR data were collected for these calculations and results according to the scheme mentioned in section 4.4.1. Polarization of DMMP with glycerol and D_2O mixture as the glassing agent and at the microwave frequency of 94.080 GHz resulted in a 2301 fold signal enhancement and a corresponding polarization buildup of 2.2%. Figure 5.8 shows the intensity in the arbitrary units of the highest hyperpolarized spectrum obtained with a single RF pulse of 25 degrees. Figure 5.9 gives a comparison of the intensity enhancement (intensities are represented in logarithmic scale) of the hyperpolarized signal as compared to the thermal equilibrium signal. Figure 5.7 shows the T_1 weighted decay of the hyperpolarization signal with time. Each signal was acquired using a single scan with a repetition time of 2 seconds. The hyperpolarized signal is available for almost 40 seconds after the insertion of the sample in the scanner.

Table 5.2 Polarization enhancement with OX063 - case 2 results

Enhancement	Percent Polarization buildup	Polarization of hyperpolarized signal	Polarization of thermal equilibrium signal
2301 folds	2.15%	0.0215	9.34e-06

Time (s)

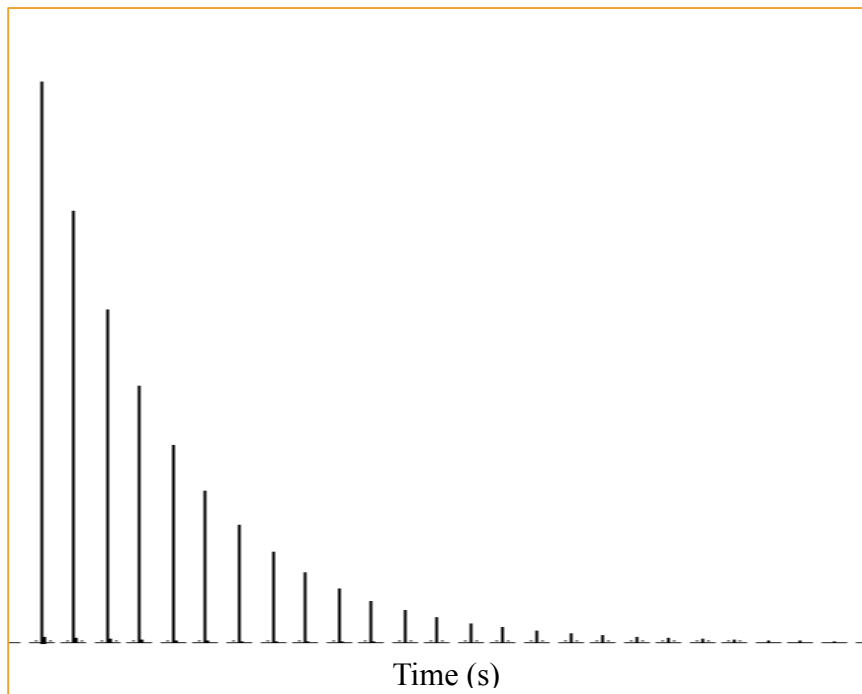Figure 5.7 T_1 weighted decay of the hyperpolarized signal obtained with OX063-case 2. Each signal was acquired using a single scan with a repetition time of 2 seconds. The hyperpolarized signal is available for almost 40 seconds after the insertion of the sample in the scanner.
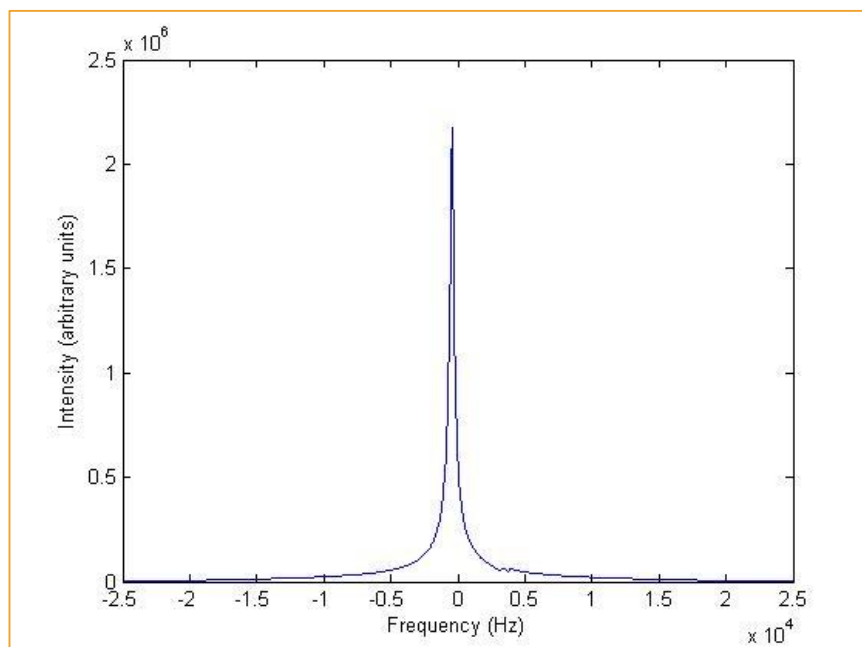
Figure 5.8 Highest hyperpolarized spectrum obtained with OX063-case 2. The spectrum was obtained with a single RF pulse of 25 degree

45
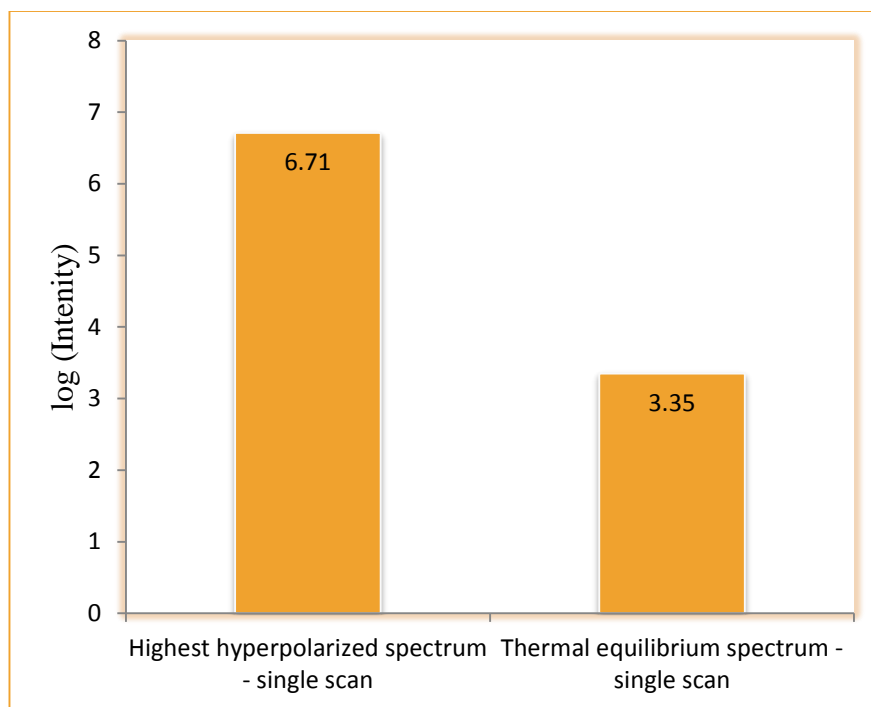
Figure 5.9 Intensity comparison between the highest hyperpolarized spectrum and thermal equilibrium spectrum obtained with OX063-case 2. The Intensities are represented on a logarithmic scale.

5.3.1.3 Case 3: Glassing Agent: Glycerol/ Deionized (dI) H2O Mixture and Microwave Irradiation Frequency: 94.080 GHz

The NMR data was collected for these calculations and results according to the scheme mentioned in section 4.4.1. Polarization of DMMP with glycerol and dI H_2O mixture as the glassing agent and at the microwave frequency of 94.080 GHz resulted in a 535 fold signal enhancement and a corresponding polarization buildup of 0.5%. Figure 5.11 shows the intensity in the arbitrary units of the highest hyperpolarized spectrum obtained with a single RF pulse of 25 degrees. Figure 5.12 gives a comparison of the logarithmic intensity enhancement of the hyperpolarized signal as compared to the thermal equilibrium signal. Figure 5.10 shows the T_1-weighted decay of the hyperpolarization signal with time. Each signal was acquired using a single scan with a repetition

time of 2 seconds. The hyperpolarized signal is available for almost 40 seconds after the insertion of the sample in the scanner.

Table 5.3 Polarization enhancement with OX063 − case 3 results

Enhancement	Percent Polarization buildup	Polarization of hyperpolarized signal	Polarization of thermal equilibrium signal
535 folds	0.5%	0.0050	9.34e-06
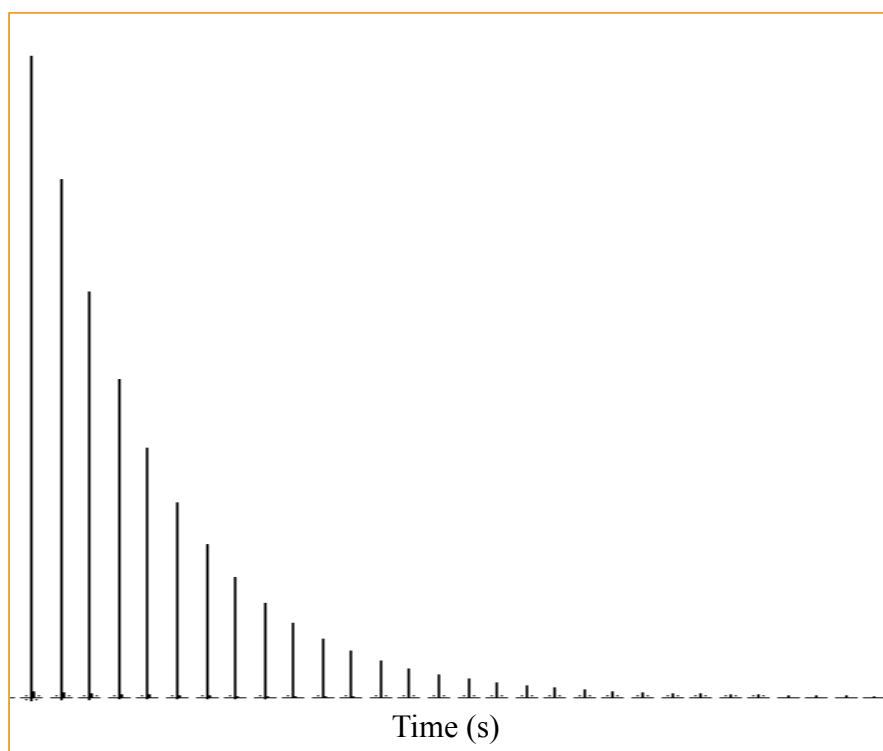
Figure 5.10 T_1 weighted decay of the hyperpolarized signal obtained with OX063-case 3. Each signal was acquired using a single scan with a repetition time of 2 seconds. The hyperpolarized signal is available for almost 40 seconds after the insertion of the sample in the scanner.
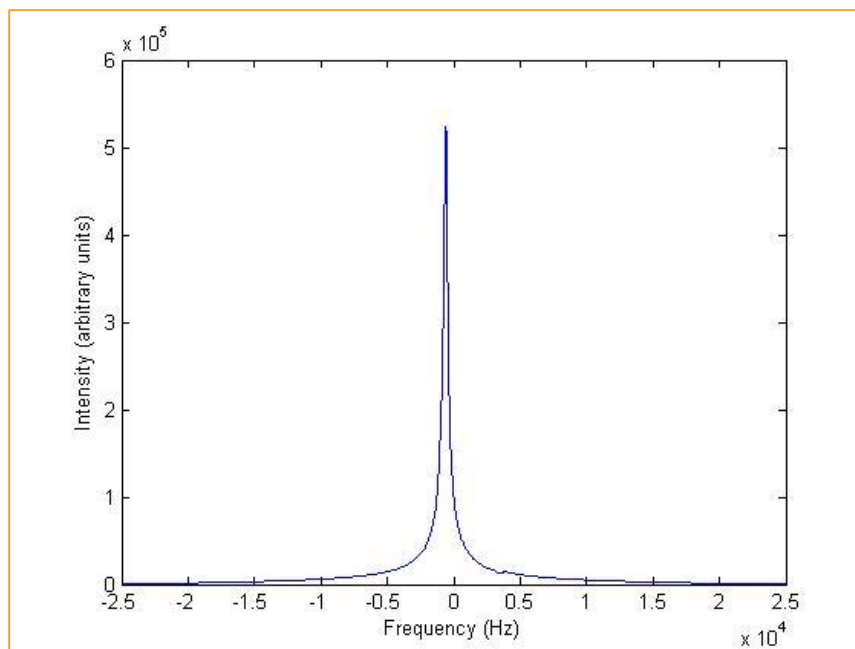
Figure 5.11 Highest hyperpolarized spectrum obtained with OX063-case 3. The spectrum was obtained with a single RF pulse of 25 degrees.
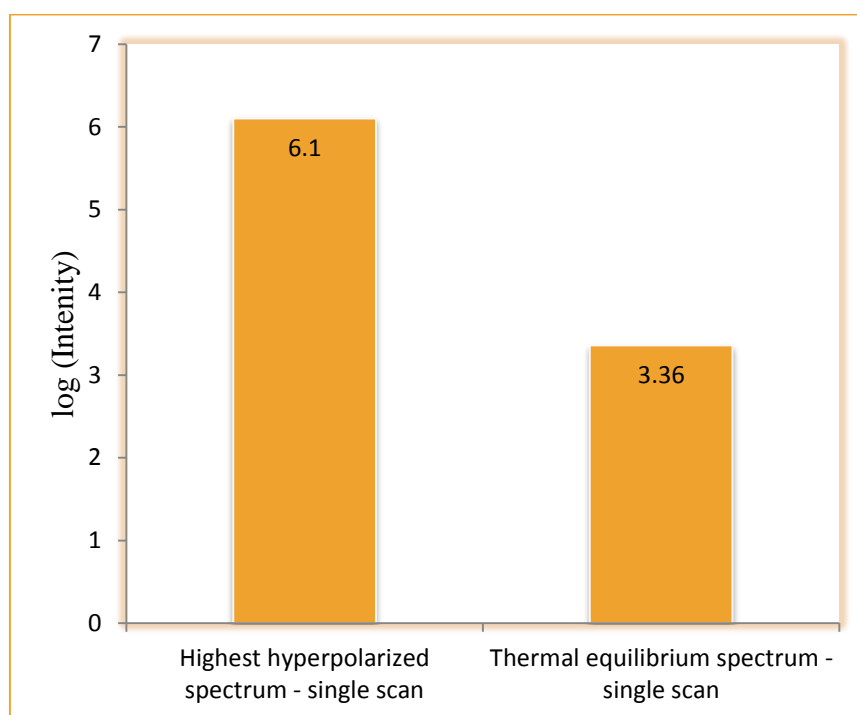
Figure 5.12 Intensity comparison between the highest hyperpolarized spectrum and thermal equilibrium spectrum obtained with OX063-case 3. The Intensities are represented on a logarithmic scale.

5.3.2 Polarization Enhancement with Radical TEMPO

5.3.2.1 Case 1: Glassing Agent: Glycerol/D₂O Mixture and Microwave Irradiation

Frequency: 94.100 GHz

The NMR data were collected for these calculations and results according to the scheme mentioned in section 4.4.1. Polarization of DMMP with glycerol and D_2O mixture as the glassing agent and at the microwave frequency of 94.100 GHz resulted in a 767.1 fold signal enhancement and a corresponding polarization buildup of 0.72%. Figure 5.14 shows the intensity in the arbitrary units of the highest hyperpolarized spectrum obtained with a single RF pulse of 25 degrees. Figure 5.15 gives a comparison of the logarithmic intensity enhancement of the hyperpolarized signal as compared to the thermal equilibrium signal. Figure 5.13 shows the T_1 weighted decay of the hyperpolarization signal with time. Each signal was acquired using a single scan with a repetition time of 2 seconds. The hyperpolarized signal is available for almost 40 seconds after the insertion of the sample in the scanner.

Table 5.4 Polarization enhancement with TEMPO - case 1 results

| Enhancement	Percent Polarization buildup	Polarization of hyperpolarized signal	Polarization of thermal equilibrium signal
767 folds	0.72%	0.0072	9.34e-06

Time (s)
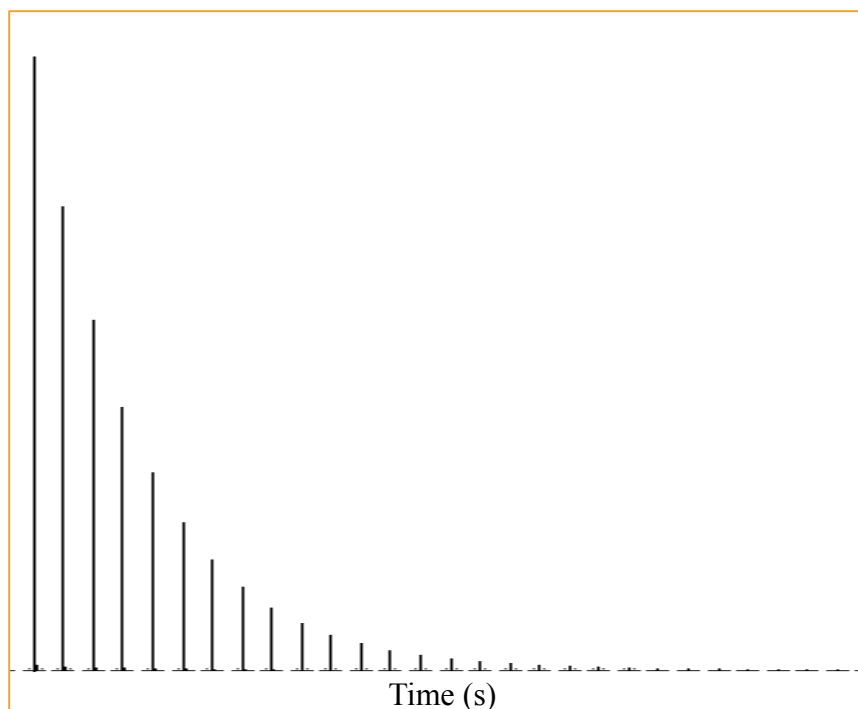
Figure 5.13 T_1 weighted decay of the hyperpolarized signal obtained with TEMPO-case 1. Each signal was acquired using a single scan with a repetition time of 2 seconds. The hyperpolarized signal is available for almost 40 seconds after the insertion of the sample in the scanner.
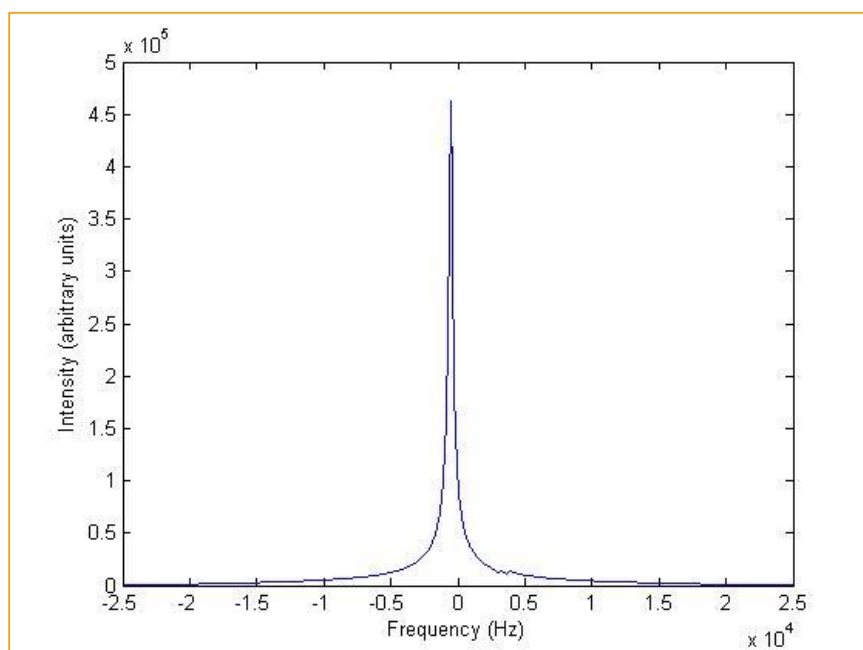
Figure 5.14 Highest hyperpolarized spectrum obtained with TEMPO-case 1. The spectrum was obtained with a single RF pulse of 25 degrees.

Figure 5.15 Intensity comparison between the highest hyperpolarized spectrum and thermal equilibrium spectrum obtained with TEMPO-case 1. The Intensities are represented on a logarithmic scale.

5.3.2.2 Case 2: Glassing Agent: Glycerol/D$_2$O Mixture and Microwave Irradiation

Frequency: 94.174 GHz

The NMR data was collected for these calculations and results according to the scheme mentioned in section 4.4.1. Polarization of DMMP with glycerol and D$_2$O mixture as the glassing agent and at the microwave frequency of 94.174 GHz resulted in a 580 fold signal enhancement and a corresponding polarization buildup of 0.54%. Figure 5.17 shows the intensity in the arbitrary units of the highest hyperpolarized spectrum obtained with a single RF pulse of 25 degrees. Figure 5.18 gives a comparison of the logarithmic intensity of the hyperpolarized signal as compared to the thermal equilibrium signal. Figure 5.16 shows the T$_1$ weighted decay of the hyperpolarization signal with 'hyperpolarized signal is available for almost 40 seconds after the insertion of the sample in the scanner.

51

Table 5.5 Polarization enhancement with TEMPO - case 2 results

| Enhancement	Percent Polarization buildup	Polarization of hyperpolarized signal	Polarization of thermal equilibrium signal
580 folds	0.54%	0.0054	9.34e-06

Time (s)
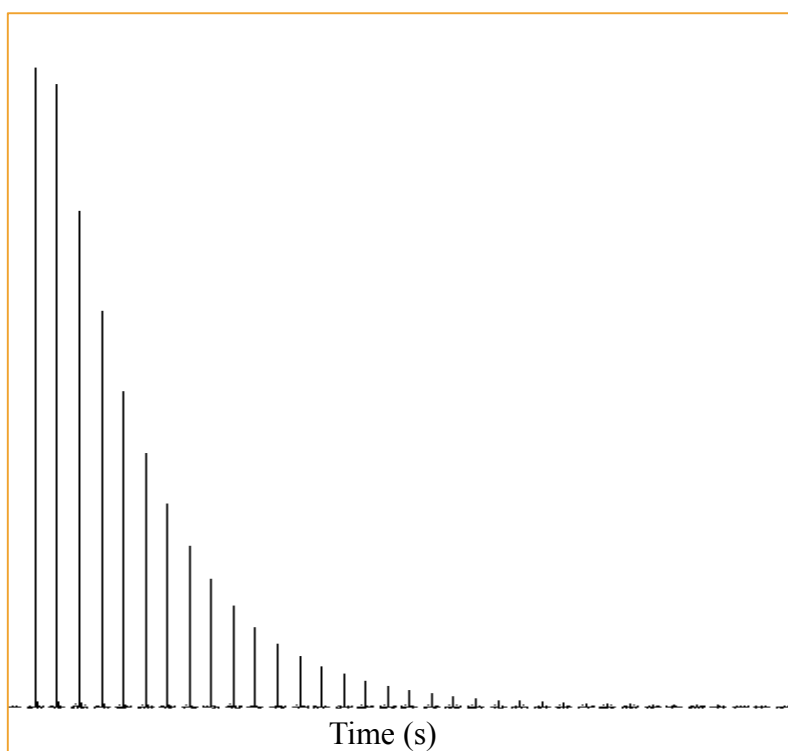
Figure 5.16 T_1 weighted decay of the hyperpolarized signal obtained with TEMPO-case 2. Each signal was acquired using a single scan with a repetition time of 2 seconds. The hyperpolarized signal is available for almost 40 seconds after the insertion of the sample in the scanner
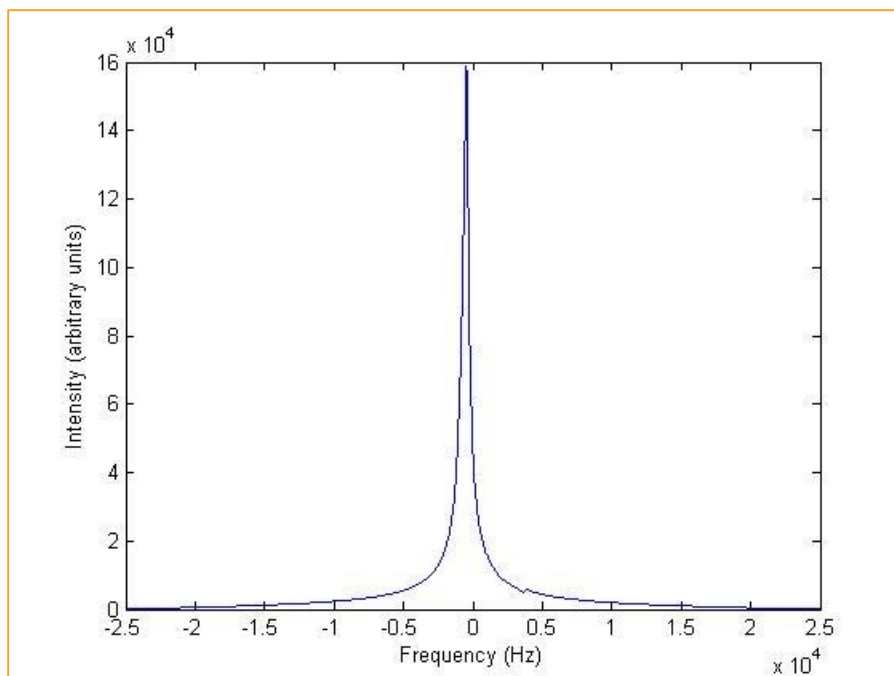
Figure 5.17 Highest hyperpolarized spectrum obtained with TEMPO-case 2. The spectrum was obtained with a single RF pulse of 25 degrees.
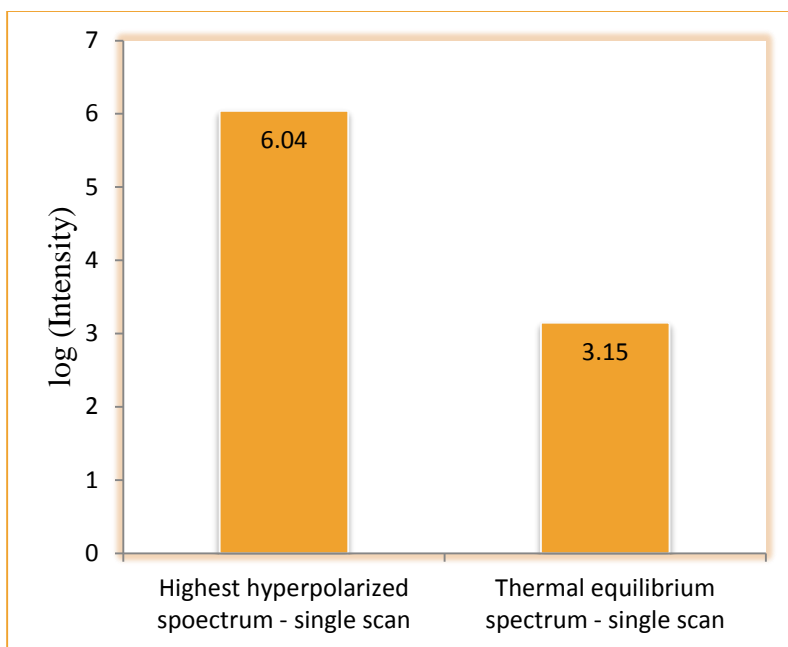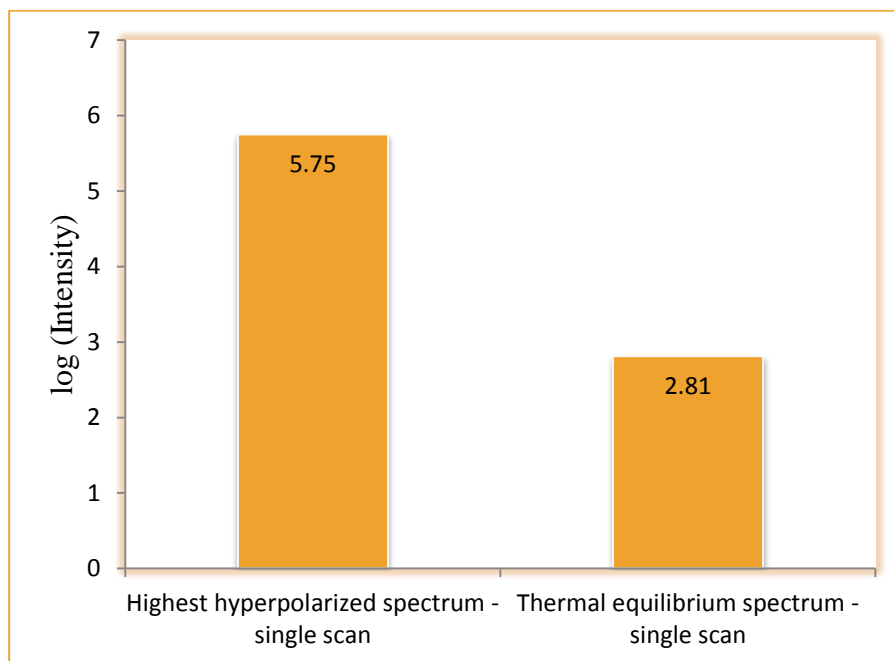

Figure 5.18 Intensity comparison between the highest hyperpolarized spectrum and thermal equilibrium spectrum obtained with TEMPO-case 2. The Intensities are represented on a logarithmic scale.

5.4 T_1 Relaxation Time Measurement for Hyperpolarized DMMP
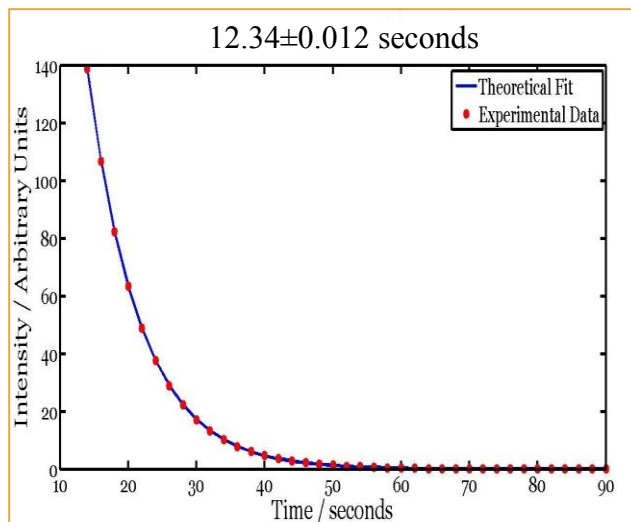
Figure 5.19 T_1 relaxation time for hyperpolarized DMMP

The T_1 relaxation time was calculated for the hyperpolarization of the DMMP with radical OX063, glassing matrix of glycerol/D_2O and at microwave frequency of 94.080 GHz. The sample preparation and data acquisition was done in the manner described above. Data were analyzed via in-house MATLAB routine and T_1 relaxation time was calculated according to the following equation:

$$I(n*TR) = M_z \sin(flipangle)\ \cos(flipangle)^{\wedge}(n\text{-}1)\ \exp(\text{-}(n\text{-}1).*TR/(T_1)) \qquad 5.1$$

whereas n is the number of the hyperpolarized spectra used for the calculation, in this case 56. M is the longitudinal magnetization or the total available hyperpolarization and TR is the time delay between each spectrum acquisition, in this case 2 s. The flip angle used was 25 degrees. As can be seen from the equation, the intentisities of the hyperpolarized spectra were compensated for the losses due to both the TR (time delay between each acquisition) and the flip angle. As shown by

the figure 5.19, the T_1 relaxation time for the hyperpolarized DMMP in solution state was calculated to be around 12 s.

5.5 Gradient Echo Multi-Slice Imaging with Hyperpolarized DMMP Phantom

Figure 5.20 Gradient echo multi-slice images of hyperpolarized DMMP phantom. The intensity in each panel is scaled to maximize the image, rather than to preserve a consistent relative intensity across images.

A GEMS imaging experiment was performed on the hyperpolarized DMPP sample. 4 mL of the sample was collected in a clear plastic polymer based tube of 5 mm outer diameter and was in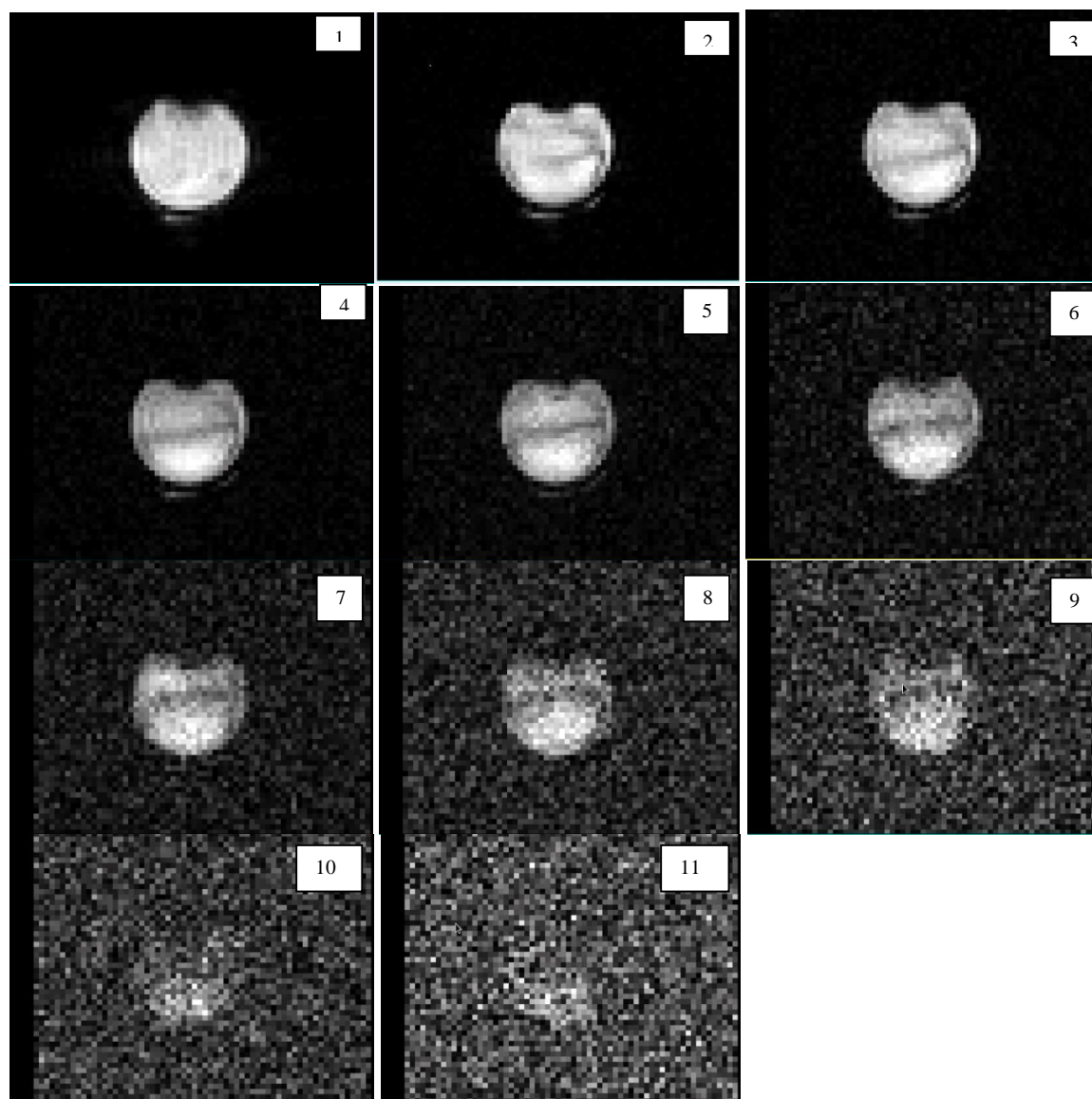serted in the RF coil placed in the MR scanner. Axial section images shown in figure 4.20 were acquired using the imaging parameters discussed in section 4.4.2.1.

Each GEMS sequence was alternated with a single pulse sequence (data not shown) to confirm the presence of a decaying hyperpolarized signal, since a single RF pulse without gradients generates a much stronger overall signal compared to 2D imaging. The flip angle used for the single pulse sequence was also 10 degrees. Time delay between each image acquisition was almost 3 s, therefore, it is evident from that the hyperpolarized signal was available for around 30 s before it decayed completely.

5.6 Gradient Echo Multi-Slice Imaging and Single Pulse Spectroscopy with Hyperpolarized DMMP in-vivo

Figure 5.21 shows the coronal section anatomical images used for the registration of the hyperpolarized DMMP images. As a slice thickness of 30 mm was used to acquire the hyperpolarized DMMP image, all of the anatomical images shown in the figure 4.19 contributed in the intensity of the total hyperpolarized signal. Figure 5.23 shows the hyperpolarized DMMP image registered with the anatomical image. The hyperpolarized DMMP image shown in the figure was obtained about 4-5 seconds after the injection. The images acquired before it and after the injection did not show hyperpolarized DMMP. Figure 5.22 shows the single scan spectra of hyperpolarized DMMP. The hyperpolarization had decayed completely after 5 single scan acquisitions of spectra. The right most peak in the spectrum appears to be coming from the endogenous phosphorous as the figure 5.22(a) shows that peak only and was obtained before the hyperpolarized DMMP had reached the blood stream of the animal. The middle and the left most

56

peaks in the spectra are both coming from the hyperpolarized DMMP, the presence of the 2 hyperpolarized peaks is likely due to susceptibility effects of the local environment inside the animal.

Using single pulse sequence alternately with GEMS, both on the ^{31}P channel, allowed for the observation of the temporal delivery of hyperpolarized DMMP to the animal along with a spatial distribution of agent. In fact, it is interesting to note that the NMR tube filled with DMMP (used as a reference) is not visible in the hyperpolarized images as they were acquired with a single average; whereas the tube is clearly visible in GEMS ^{31}P images that were acquired with 128 averages (data not shown). This exemplifies the potential advantages of hyperpolarization where a neat solvent with nearly 100% ^{31}P abundance does not show up in an image with a single scan at these low spatial resolutions.
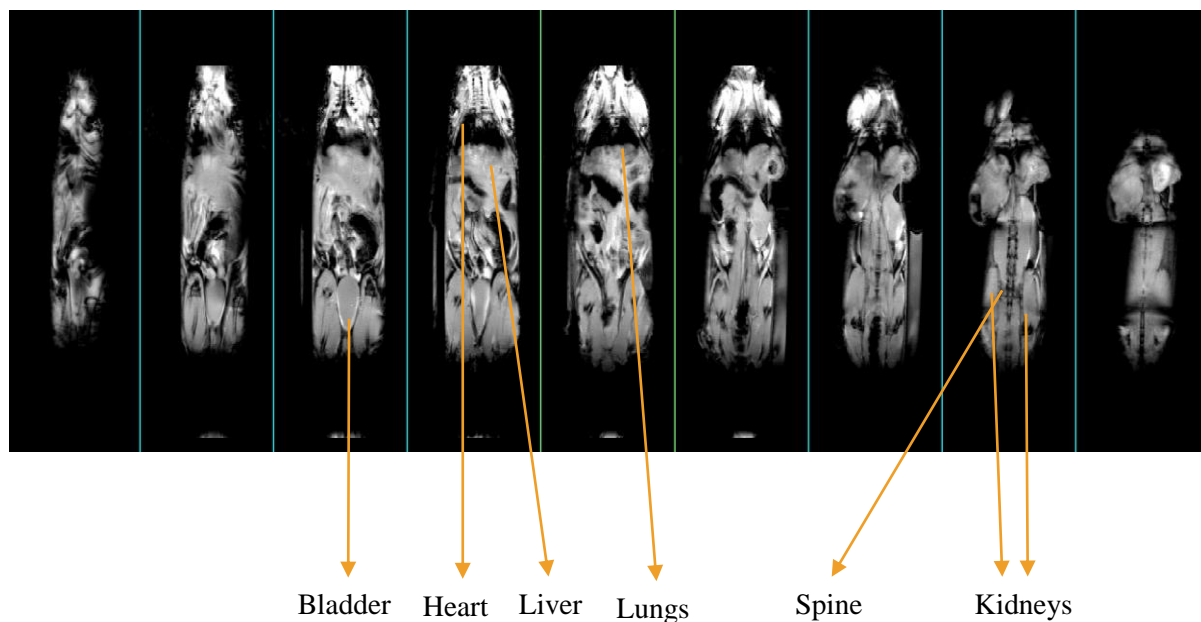
Figure 5.21 Coronal section anatomical images used for the registration of the hyperpolarized DMMP images. An NMR tube filled with DMMP for spatial ^{31}P reference is visible in the image.
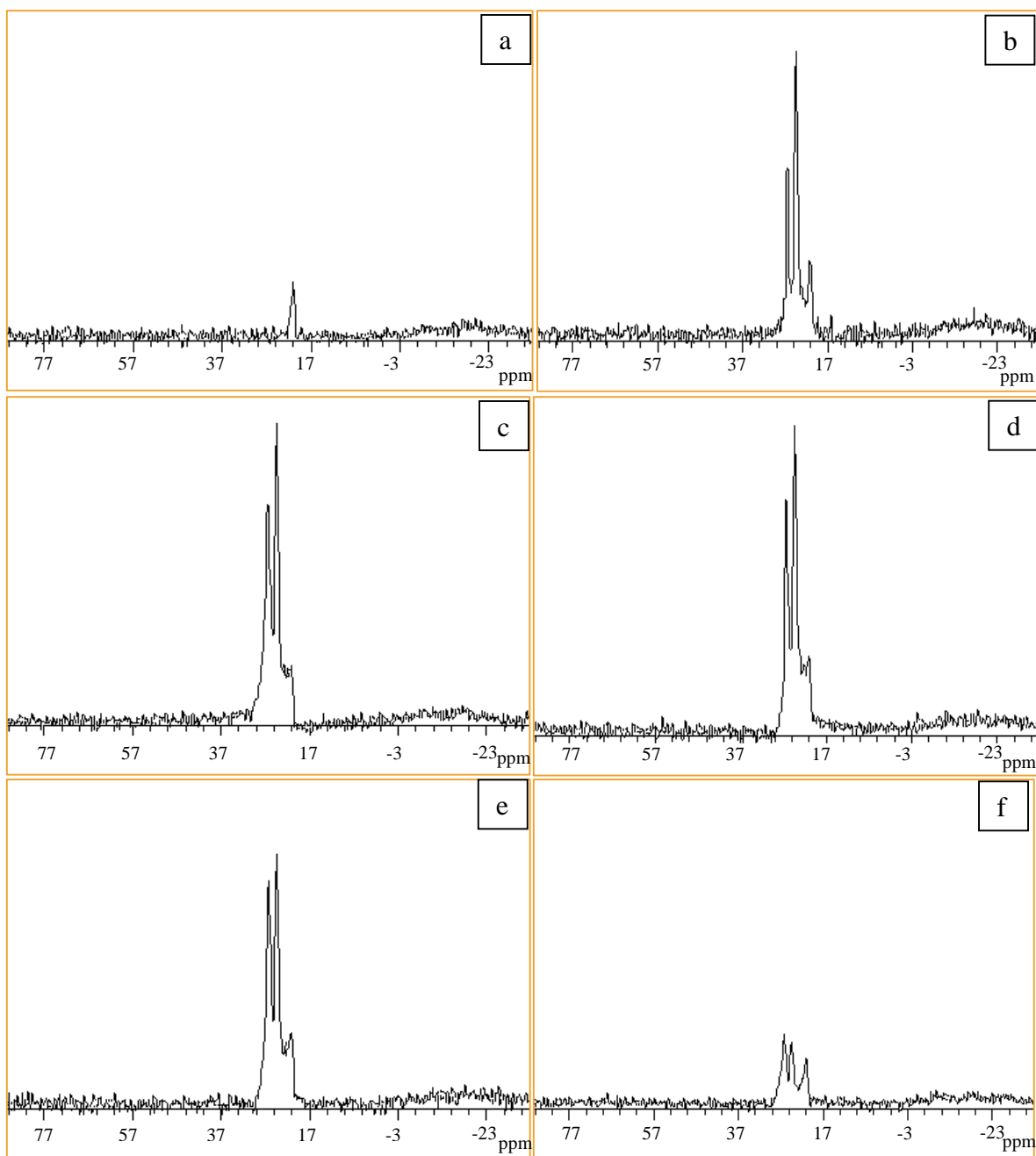
Figure 5.22 Single scan spectra of hyperpolarized DMMP in-vivo. (a) Spectrum of endogenous phosphorous. (b) First hyperpolarized DMMP spectrum. (c) Second hyperpolarized DMMP spectrum. (d) Third hyperpolarized DMMP spectrum. (e) Fourth hyperpolarized DMMP spectrum. (f) Fifth and last hyperpolarized spectrum. The hyperpolarization signal had completely decayed at this time (about 5 seconds after the injection).
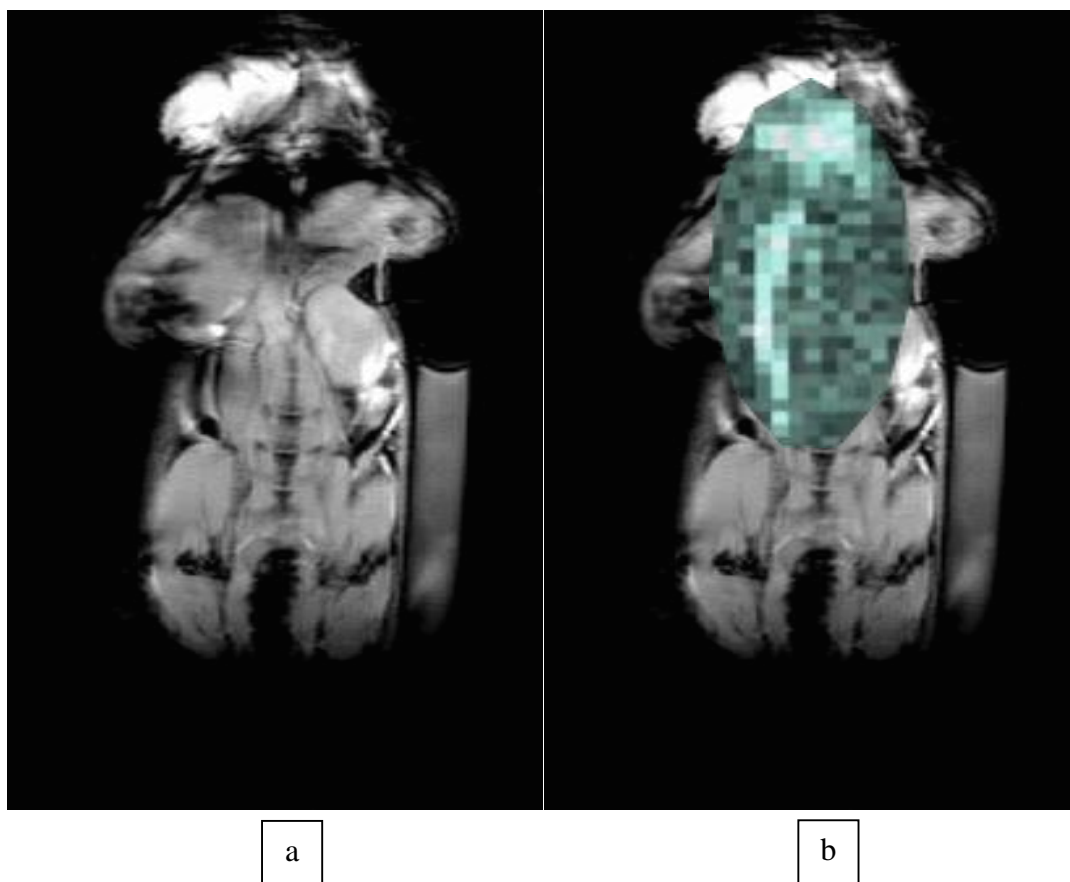
Figure 5.23 Hyperpolarized DMMP in-vivo image. (a) The coronal section anatomical image used for the registration. (b) Hyperpolarized DMMP image registered with the anatomical image.

These results demonstrate the first ever application of ^{31}P DNP in phosphonates and indicate the potential application of hyperpolarized DMMP in the functional imaging and spectroscopic studies. In this study, only 1 image of the hyperpolarized DMMP could be acquired 5-6 s after the injection and before the hyperpolarization signal decay. The image indicates that DMMP was present in the blood stream and some of it diffused into the heart. Due to a very fast T_1 relaxation rate, multiple images could not be acquired using the experimental set up discussed above at this time. Further investigations to improve the pulse sequences and to increase the T_1 relaxation time would definitely provide better results and help modeling the delivery and subsequent diffusion of DMMP in-vivo more accurately.

One other challenge is the limited amount of the sample that can be injected into the animal. The images and signal shown above were acquired using only 7.8 µl of the hyperpolarized DMMP which is way below the lethal concentration that could be administered in the animal. This quantity is somewhat limited by the maximum sample volume that can be polarized at a given time. Further investigations to explore the maximum amount of the sample that can be polarized and dissolved with the minimum amount of dissolution solvent to dissolve all of the sample would potentially increase the total injectable amount and yield stronger signal in the animal.

The chemical shift anisotropy effects are more pronounced at higher magnetic field strengths which result in a faster T_1 relaxation rate of the hyperpolarized signal. These effects are reduced at lower magnetic field strengths, therefore, the hyperpolarized signal is expected to be seen for longer times at the magnetic field strengths used in the clinical settings (typically 1.5T or 3 T).

5.7 Conclusions

In this work, I have successfully demonstrated and optimized the dynamic nuclear polarization in DMMP. The largest polarization enhancements were achieved when DMMP was hyperpolarized with the radical OX063 at 94.080 GHz, glassing mixture of D_2O and glycerol in a volume ratio of 1:1 and dissolved with D_2O.

The hyperpolarized signal, although short lived, was successfully delivered and imaged in-vivo. The low intensity of the hyperpolarized DMMP images in-vivo as compared to the hyperpolarized images of the phantom is associated with a number of factors that play a part in enhancing the T_1 relaxation rate as well as decreasing the signal intensity. A few of them include limited amount of the hyperpolarized substance that could be injected in the animal, the time it takes for the hyperpolarized substance to reach the circulatory system, susceptibility due to the paramagnetic

60

species, for example air, present in the animal, electrolytes that decrease the sensitivity of the RF coils, etc.

This work concludes that hyperpolarized DMMP is a potential candidate for in-vivo imaging and spectroscopic studies. However, further optimization of the imaging sequences, enhancement of the T_1 relaxation time and (or) possible increase in the polarization buildup is required and would yield better results.

References

1. Overhauser, A. W., Polarization of Nuclei in Metals. *Physical Review* **1953,** *92* (2), 411-415.

2. Carver, T. R.; Slichter, C. P., Experimental Verification of the Overhauser Nuclear Polarization Effect. *Physical Review* **1956,** *102* (4), 975-980.

3. Carver, T. R.; Slichter, C. P., Polarization of Nuclear Spins in Metals. *Physical Review* **1953,** *92* (1), 212-213

4. Kelly, A. E.; Ou, H. D.; Withers, R.; Dotsch, V., Low-conductivity buffers for high-sensitivity NMR measurements. *J Am Chem Soc* **2002,** *124* (40), 12013-9.

5. Kovacs, H.; Moskau, D.; Spraul, M., Cryogenically cooled probes—a leap in NMR technology. *Progress in Nuclear Magnetic Resonance Spectroscopy* **2005,** *46* (2–3), 131-155.

6. Schneider-Muntau, H. J., High field NMR magnets. *Solid State Nucl Magn Reson* **1997,** *9* (1), 61-71.

7. Ardenkjaer-Larsen, J. H.; Fridlund, B.; Gram, A.; Hansson, G.; Hansson, L.; Lerche, M. H.; Servin, R.; Thaning, M.; Golman, K., Increase in signal-to-noise ratio of > 10,000 times in liquid-state NMR. *Proceedings of the National Academy of Sciences of the United States of America* **2003,** *100* (18), 10158-63

8. Brindle, K., New approaches for imaging tumour responses to treatment. *Nature reviews. Cancer* **2008,** *8* (2), 94-107.

9. Lingwood, M. D.; Han, S., Dynamic nuclear polarization of 13C in aqueous solutions under ambient conditions. *Journal of magnetic resonance (San Diego, Calif. : 1997)* **2009,** *201* (2), 137-45.

10. Wenckebach, W. T., The Solid Effect. *Appl Magn Reson* **2008,** *34* (3-4), 227-235

11. De Graaf, R. A., *In vivo NMR spectroscopy [electronic resource] : principles and techniques / Robin de Graaf.* Chichester, West Sussex, England ; Hoboken, NJ : John Wiley & Sons, c2007. 2nd ed.: 2007.

12. Goldman, M., Overview of Spin Temperature, Thermal Mixing and Dynamic Nuclear Polarization. *Appl Magn Reson* **2008,** *34* (3-4), 219

13. Abragam, A.; Goldman, M., Principles of dynamic nuclear polarization. *Rep. Prog. Phys.* **1978,** *41*, 395-467.

14. Maly, T.; Debelouchina, G. T.; Bajaj, V. S.; Hu, K. N.; Joo, C. G.; Mak-Jurkauskas, M. L.; Sirigiri, J. R.; van der Wel, P. C.; Herzfeld, J.; Temkin, R. J.; Griffin, R. G., Dynamic nuclear polarization at high magnetic fields.*J Chem Phys* **2008,** *128* (5), 052211

15. http://www.oxford-instruments.com/products/spectrometers/nuclear-magnetic-resonance-nmr/hypersense

16. Day, I. J.; Mitchell, J. C.; Snowden, M. J.; Davis, A. L., Applications of DNP-NMR for the measurement of heteronuclear T1 relaxation times. *Journal of magnetic resonance (San Diego, Calif. : 1997)* **2007,** *187* (2), 216-24.

17. Zhao, L.; Mulkern, R.; Tseng, C. H.; Williamson, D.; Patz, S.; Kraft, R.; Walsworth, R. L.; Jolesz, F. A.; Albert, M. S., Gradient-echo imaging considerations for hyperpolarized 129Xe MR. *Journal of magnetic resonance. Series B* **1996,** *113*, 179-83.

18. Zeng, H.; Bowen, S.; Hilty, C., Sequentially acquired two-dimensional NMR spectra from hyperpolarized sample. *Journal of magnetic resonance (San Diego, Calif. : 1997)* **2009,** *199* (2), 159-65.

19. Atsarkin, V. A., Dynamic nuclear polarization: Yesterday, today, and tomorrow. *Journal of Physics: Conference Series* **2011,** *324* (1), 012003.

20. Levitt, M. H., *Spin Dynamics: Basics of Nuclear Magnetic Resonance*. Wiley: 2001.

21. Bloch, F., Nuclear Induction. *Physical Review* **1946,** *70* (7-8), 460-474.

22. Bloembergen, N., *Nuclear Magnetic Relaxation: A Reprint Volume*. W.A. Benjamin: 1961.

23. Akbey, U.; Altin, B.; Linden, A.; Ozcelik, S.; Gradzielski, M.; Oschkinat, H., Dynamic nuclear polarization of spherical nanoparticles. *Physical Chemistry Chemical Physics* **2013,** *15* (47), 20706-20716.

24. Bhujwalla, Z. M.; McCoy, C. L.; Glickson, J. D.; Gillies, R. J.; Stubbs, M., Estimations of intra- and extracellular volume and pH by 31P magnetic resonance spectroscopy: effect of therapy on RIF-1 tumours. *Br J Cancer* **1998,** *78* (5), 606-11

25. Bhattacharyya, D.; Nama, D. B.; Reynolds, S. "Deoxynucleotide Triph- osphates and Oligonucleotides by 31P DNP NMR", Oxford Instruments application note (OX63 available from OIMBL).

26. Gabellieri, C.; Reynolds, S.; Lavie, A.; Payne, G. S.; Leach, M. O.; Eykyn, T. R., Therapeutic target metabolism observed using hyperpolarized 15N choline. *J Am Chem Soc* **2008,** *130* (14), 4598-9.

27. Gallagher, F. A.; Kettunen, M. I.; Day, S. E.; Hu, D. E.; Ardenkjaer-Larsen, J. H.; Zandt, R.; Jensen, P. R.; Karlsson, M.; Golman, K.; Lerche, M. H.; Brindle, K. M., Magnetic resonance imaging of pH in vivo using hyperpolarized 13C-labelled bicarbonate. *Nature* **2008,** *453* (7197), 940-3.

28. Golman, K.; in 't Zandt, R.; Thaning, M., Real-time metabolic imaging. *Proceedings of the National Academy of Sciences of the United States of America* **2006,** *103* (30), 11270-5.

29. Golman, K.; Zandt, R. I.; Lerche, M.; Pehrson, R.; Ardenkjaer-Larsen, J. H., Metabolic imaging by hyperpolarized 13C magnetic resonance imaging for in vivo tumor diagnosis. *Cancer research* **2006,** *66* (22), 10855-60.

30. Williams, D. S.; Detre, J. A.; Leigh, J. S.; Koretsky, A. P., Magnetic resonance imaging of perfusion using spin inversion of arterial water. *Proceedings of the National Academy of Sciences of the United States of America* **1992,** *89* (1), 212-6.

31. Herscovitch, P.; Markham, J.; Raichle, M. E., Brain blood flow measured with intravenous H2(15)O. I. Theory and error analysis. *Journal of nuclear medicine : official publication, Society of Nuclear Medicine* **1983,** *24* (9), 782-9.

32. Herscovitch, P.; Raichle, M. E.; Kilbourn, M. R.; Welch, M. J., Positron emission tomographic measurement of cerebral blood flow and permeability-surface area product of water using [15O]water and [11C]butanol. *Journal of cerebral blood flow and metabolism : official journal of the International Society of Cerebral Blood Flow and Metabolism* **1987,** *7* (5), 527-42.

33. Neirinckx, R. D.; Canning, L. R.; Piper, I. M.; Nowotnik, D. P.; Pickett, R. D.; Holmes, R. A.; Volkert, W. A.; Forster, A. M.; Weisner, P. S.; Marriott, J. A.; et al., Technetium-99m d,l-HM-PAO: a new radiopharmaceutical for SPECT imaging of regional cerebral blood perfusion. *Journal of nuclear medicine : official publication, Society of Nuclear Medicine* **1987,** *28* (2), 191-202.

34. Tsuchida, T.; Yonekura, Y.; Nishizawa, S.; Sadato, N.; Tamaki, N.; Fujita, T.; Magata, Y.; Konishi, J., Nonlinearity correction of brain perfusion SPECT based on permeability-surface area product model. *Journal of nuclear medicine : official publication, Society of Nuclear Medicine* **1996,** *37* (7), 1237-41.

35. Brix, G.; Bahner, M. L.; Hoffmann, U.; Horvath, A.; Schreiber, W., Regional blood flow, capillary permeability, and compartmental volumes: measurement with dynamic CT--initial experience. *Radiology* **1999,** *210* (1), 269-76.

36. Gur, D.; Yonas, H.; Herbert, D.; Wolfson, S. K.; Kennedy, W. H.; Drayer, B. P.; Gray, J., Xenon enhanced dynamic computed tomography: multilevel cerebral blood flow studies. *Journal of computer assisted tomography* **1981,** *5* (3), 334-40.

37. Seifert, H.; Blass, G.; Leetz, H. K.; Voges, M., The radiation exposure of the patient from stable-xenon computed tomography. *Br J Radiol* **1995,** *68* (807), 301-5.

38. Ostergaard, L.; Sorensen, A. G.; Kwong, K. K.; Weisskoff, R. M.; Gyldensted, C.; Rosen, B. R., High resolution measurement of cerebral blood flow using intravascular tracer bolus passages. Part II: Experimental comparison and preliminary results. *Magnetic resonance in medicine : official journal of the Society of Magnetic Resonance in Medicine / Society of Magnetic Resonance in Medicine* **1996,** *36* (5), 726-36.

39. Pekar, J.; Ligeti, L.; Ruttner, Z.; Lyon, R. C.; Sinnwell, T. M.; van Gelderen, P.; Fiat, D.; Moonen, C. T.; McLaughlin, A. C., In vivo measurement of cerebral oxygen consumption and blood flow using 17O magnetic resonance imaging. *Magnetic resonance in medicine : official journal of the Society of Magnetic Resonance in Medicine / Society of Magnetic Resonance in Medicine* **1991,** *21* (2), 313-9.

40. Detre, J. A.; Subramanian, V. H.; Mitchell, M. D.; Smith, D. S.; Kobayashi, A.; Zaman, A.; Leigh, J. S., Jr., Measurement of regional cerebral blood flow in cat brain using intracarotid 2H2O and 2H NMR imaging. *Magnetic resonance in medicine : official journal of the Society of Magnetic Resonance in Medicine / Society of Magnetic Resonance in Medicine* **1990,** *14* (2), 389-95.

41. Tofts, P. S.; Brix, G.; Buckley, D. L.; Evelhoch, J. L.; Henderson, E.; Knopp, M. V.; Larsson, H. B.; Lee, T. Y.; Mayr, N. A.; Parker, G. J.; Port, R. E.; Taylor, J.; Weisskoff, R. M., Estimating kinetic parameters from dynamic contrast-enhanced T(1)-weighted MRI of a diffusable tracer: standardized quantities and symbols. *Journal of magnetic resonance imaging : JMRI* **1999,** *10* (3), 223-32.

42. Day, S. E.; Kettunen, M. I.; Gallagher, F. A.; Hu, D. E.; Lerche, M.; Wolber, J.; Golman, K.; Ardenkjaer-Larsen, J. H.; Brindle, K. M., Detecting tumor response to treatment using hyperpolarized 13C magnetic resonance imaging and spectroscopy. *Nature medicine* **2007,** *13* (11), 1382-7.

43. Chen, A. P.; Albers, M. J.; Cunningham, C. H.; Kohler, S. J.; Yen, Y. F.; Hurd, R. E.; Tropp, J.; Bok, R.; Pauly, J. M.; Nelson, S. J.; Kurhanewicz, J.; Vigneron, D. B., Hyperpolarized C-13 spectroscopic imaging of the TRAMP mouse at 3T-initial experience. *Magnetic resonance in medicine : official journal of the Society of Magnetic Resonance in Medicine / Society of Magnetic Resonance in Medicine* **2007,** *58* (6), 1099-106.

44. Albers, M. J.; Bok, R.; Chen, A. P.; Cunningham, C. H.; Zierhut, M. L.; Zhang, V. Y.; Kohler, S. J.; Tropp, J.; Hurd, R. E.; Yen, Y. F.; Nelson, S. J.; Vigneron, D. B.; Kurhanewicz, J., Hyperpolarized 13C lactate, pyruvate, and alanine: noninvasive biomarkers for prostate cancer detection and grading. *Cancer research* **2008,** *68* (20), 8607-15.

45. Ward, C. S.; Venkatesh, H. S.; Chaumeil, M. M.; Brandes, A. H.; Vancriekinge, M.; Dafni, H.; Sukumar, S.; Nelson, S. J.; Vigneron, D. B.; Kurhanewicz, J.; James, C. D.; Haas-Kogan, D. A.; Ronen, S. M., Noninvasive detection of target modulation following phosphatidylinositol 3-kinase inhibition using hyperpolarized 13C magnetic resonance spectroscopy. *Cancer research* **2010,** *70* (4), 1296-305.

46. Merritt, M. E.; Harrison, C.; Kovacs, Z.; Kshirsagar, P.; Malloy, C. R.; Sherry, A. D., Hyperpolarized (89)Y offers the potential of direct imaging of metal ions in biological systems by magnetic resonance. *J Am Chem Soc* **2007,** *129* (43), 12942-3.

47. von Morze, C.; Larson, P. E.; Hu, S.; Keshari, K.; Wilson, D. M.; Ardenkjaer-Larsen, J. H.; Goga, A.; Bok, R.; Kurhanewicz, J.; Vigneron, D. B., Imaging of blood flow using hyperpolarized [(13)C]urea in preclinical cancer models. *Journal of magnetic resonance imaging : JMRI* **2011,** *33* (3), 692-7.

Appendices

Appendix A Copyright Permission

The following is the copyright permission for use of figure 3.37 in chapter 3.

**JOHN WILEY AND SONS LICENSE
TERMS AND CONDITIONS**

Jun 10, 2014

This is a License Agreement between Roha Afzal ("You") and John Wiley and Sons ("John Wiley and Sons") provided by Copyright Clearance Center ("CCC"). The license consists of your order details, the terms and conditions provided by John Wiley and Sons, and the payment terms and conditions.

All payments must be made in full to CCC. For payment instructions, please see information listed at the bottom of this form.

License Number	3405710612066
License date	Jun 10, 2014
Licensed content publisher	John Wiley and Sons
Licensed content publication	Wiley oBooks
Licensed content title	Basic Principles
Book title	In Vivo NMR Spectroscopy, 2nd Edition
Licensed copyright line	Copyright © 2007 John Wiley & Sons, Ltd
Licensed content author	Robin A. de Graaf
Licensed content date	Nov 1, 2007
Start page	1
End page	42
Type of use	Dissertation/Thesis
Requestor type	University/Academic
Format	Print and electronic
Portion	Figure/table
Number of figures/tables	3
Original Wiley figure/table number(s)	figure 1.1 figure 1.2 figure 3.37
Will you be translating?	No
Title of your thesis / dissertation	Dissolution DNP in 31P nucleus in phosphonates for functional imaging and spectroscopic applications in-vitro and in-vivo
Expected completion date	Jun 2014
Expected size (number of pages)	50
Total	0.00 USD
Terms and Conditions	

TERMS AND CONDITIONS

Appendix B IACUC Approval

USF UNIVERSITY OF SOUTH FLORIDA

RESEARCH INTEGRITY AND COMPLIANCE
INSTITUTIONAL ANIMAL CARE & USE COMMITTEE

MEMORANDUM

TO:	Robert Gillies , Ph.D.
FROM:	Farah Moulvi, MSPH, IACUC Coordinator Institutional Animal Care & Use Committee Division of Research Integrity & Compliance
DATE:	1/8/2014
PROJECT TITLE:	Hyperpolarized MRI in Cancer Imaging and Therapy
FUNDING SOURCE:	Huizinga Foundation Funds
IACUC PROTOCOL #:	R IS00000093
PROTOCOL STATUS:	**APPROVED**

Your request for continuation of this study was received and will be reported to the Institutional Animal Care and Use Committee (IACUC). The IACUC acknowledges that this study is currently on going as previously approved. Please be advised that **continuation of this study is in effect for a one-year period beginning 3/28/2014:**

Please take note of the following

• **IACUC approval is granted for a one-year period at the end of which, an annual renewal form must be submitted for years two (2) and three (3) of the protocol through the eIACUC system.** After three years all continuing studies must be completely re-described in a new electronic application and submitted to IACUC for review.

• **All modifications to the IACUC-Approved Protocol must be approved by the IACUC prior to initiating the modification.** Modifications can be submitted to the IACUC for review and approval as an Amendment or Procedural Change through the eIACUC system. These changes must be within the scope of the original research hypothesis, involve the original species and justified in writing. Any change in the IACUC-approved protocol that does not meet the latter definition is considered a major protocol change and requires the submission of a new application.